batteries

Review

Hydrogel Polymer Electrolytes for Aqueous Zinc-Ion Batteries: Recent Progress and Remaining Challenges

Zhaoxuan Zhu [1], Sihan Xiong [2], Jing Li [3], Lixin Wang [1], Xiaoning Tang [1], Long Li [1], Qi Sun [1], Yan Shi [1,*] and Jiaojing Shao [1,*]

[1] School of Materials and Metallurgy, Guizhou University, Guiyang 550025, China; gs.zhuzx22@gzu.edu.cn (Z.Z.); gs.lxwang24@gzu.edu.cn (L.W.); xntang@gzu.edu.cn (X.T.); lilong@gzu.edu.cn (L.L.); qsun@gzu.edu.cn (Q.S.)
[2] School of Life and Environmental Sciences, Deakin University, Melbourne 3125, Australia; s223103816@deakin.edu.au
[3] State Key Laboratory of Structural Chemistry, Fujian Institute of Research on the Structure of Matter, Chinese Academy of Sciences, Fuzhou 350002, China; lijing@fjirsm.ac.cn
* Correspondence: shiyan1262006@126.com or yshi3@gzu.edu.cn (Y.S.); shaojiao_jing@163.com (J.S.)

Abstract

Aqueous zinc-ion batteries (ZIBs) have attracted growing interest as promising candidates for large-scale and flexible energy storage due to their intrinsic safety, low cost, and environmental sustainability. However, several persistent issues—such as uncontrolled Zn dendrite growth, hydrogen evolution-induced anode corrosion, and cathode dissolution—continue to hinder their commercial deployment. To address these challenges, hydrogel polymer electrolytes (HPEs) have emerged as an effective strategy. Their unique three-dimensional polymer networks not only retain water and confine ion transport, but also provide a solid–liquid hybrid environment that enhances ionic conductivity and interfacial compatibility. These features enable HPEs to suppress side reactions and improve both electrochemical stability and mechanical adaptability, which are especially valuable for flexible ZIB devices. This review first summarizes fundamental energy storage mechanisms in aqueous ZIBs, including reversible Zn^{2+} insertion/extraction, proton co-insertion, and cathode phase evolution. It then highlights recent progress in HPE design, with emphasis on polyacrylamide (PAM), polyvinyl alcohol (PVA), and polyacrylic acid (PAA)-based systems, with strategies for dendrite suppression, interfacial regulation, and mechanical robustness. Finally, current challenges and future directions are discussed, with a forward-looking perspective on scalable fabrication methods, advanced electrolyte design, and deeper mechanistic understanding necessary to fully realize the potential of HPE-enabled aqueous ZIBs.

Keywords: hydrogel polymer electrolytes; zinc-ion batteries; energy storage mechanisms; zinc dendrite suppression; electrochemical stability; polyacrylamide; polyvinyl alcohol

Academic Editor: Claudio Gerbaldi

Received: 19 August 2025
Revised: 17 September 2025
Accepted: 13 October 2025
Published: 17 October 2025
Corrected: 5 November 2025

Citation: Zhu, Z.; Xiong, S.; Li, J.; Wang, L.; Tang, X.; Li, L.; Sun, Q.; Shi, Y.; Shao, J. Hydrogel Polymer Electrolytes for Aqueous Zinc-Ion Batteries: Recent Progress and Remaining Challenges. *Batteries* **2025**, *11*, 380. https://doi.org/10.3390/batteries11100380

1. Introduction

Amid continuous global economic growth, rapid industrialization, and population expansion, the global demand for energy continues to rise steadily. However, the supply of conventional fossil fuels—including coal, petroleum, and natural gas, all of which are non-renewable—is becoming increasingly constrained. Moreover, the carbon emissions generated by their combustion exert severe impacts on the environment [1,2]. This has created an urgent need to develop sustainable, eco-friendly, and efficient energy alternatives.

Among them, electrochemical energy storage technologies—particularly batteries—play a pivotal role in enabling the transition to renewable energy, offering both practical applicability and considerable market potential [3,4].

Lithium-ion batteries (LIBs) have emerged as the cornerstone of modern energy storage systems, effectively regulating power output and facilitating the grid integration of renewable energy. Nevertheless, their application in large-scale energy storage systems is limited by escalating raw material costs and inherent safety risks [5–7]. In contrast, aqueous zinc-ion batteries (ZIBs) have attracted significant attention due to their lower cost, intrinsic safety, and the abundance of zinc resources (approximately 300 times more abundant than lithium) [8]. By employing aqueous electrolytes, ZIBs exhibit markedly higher ionic conductivity (10–100 mS cm^{-1}) compared to the 1–10 mS cm^{-1} typically observed in LIBs with organic electrolytes. In addition, ZIBs provide a high theoretical capacity (5851 mAh cm^{-3} or 820 mAh g^{-1}), environmental compatibility, and a low standard redox potential for Zn^{2+}/Zn (−0.76 V vs. standard hydrogen electrode, SHE), making them a highly promising candidate for next-generation low-cost aqueous energy storage systems [9–11].

Despite these notable advantages, ZIBs still face several technical challenges. In particular, systems utilizing aqueous electrolytes encounter issues such as the hydrogen evolution reaction (HER) and oxygen evolution reaction (OER) [12–14], which can cause electrolyte depletion, electrode corrosion and overall performance degradation [15,16]. These parasitic reactions primarily arise from the presence of free or highly active water molecules in the electrolyte. Consequently, reducing water content or suppressing water activity has become an effective strategy to mitigate these problems [17–19].

Hydrogel polymer electrolytes (HPEs) have been identified as a critical technology to address these challenges, as they can effectively suppress cathode/anode dissolution, zinc dendrite growth, and interfacial corrosion in aqueous ZIBs [20,21]. HPEs form a three-dimensional (3D) interpenetrating network structure with continuous pores through cross-linking reactions of polymer chains, in which the water molecules are physically confined. This confined environment maintains the moisture required for ion transport while enhancing both mechanical flexibility and ion transport kinetics [22–24]. Unlike traditional liquid electrolytes, HPEs leverage the synergistic effects of chemical bonding and physical adsorption to immobilize water molecules within the polymer matrix. Such confinement preserves the high ionic conductivity characteristic of aqueous electrolytes while mitigating the interface instability problems inherent in liquid systems, thereby achieving a balance between electrochemical performance and structural stability [25]. The hydrophilic functional groups commonly present in HPEs, such as hydroxyl (-OH), carboxyl (-COOH), and amide (-$CONH_2$) groups, exhibit strong affinity for Zn^{2+} ions. Serving as active sites, these groups facilitate ion migration, improve ionic conductivity, mitigate voltage loss caused by concentration polarization, and reduce morphological changes during charge/discharge cycles [26,27]. More importantly, the well-defined ion-conducting network within HPEs effectively guides the directional migration of Zn^{2+}, promoting the formation of highly ordered ion transport pathways and ensuring uniform ion distribution. This, in turn, strongly suppresses the nucleation and growth of zinc dendrites.

In HPEs, water molecules can be broadly classified into free-state or bound-state forms. The ratio between these two forms directly influences the ionic transport properties and electrochemical stability of the electrolyte [28]. In conventional liquid electrolytes, most water exists in the free state, exhibiting high mobility and electrochemical reactivity, which readily trigger HER and lead to interfacial pH fluctuations and byproduct formation. In contrast, the strong interactions between hydrophilic functional groups and water molecules in HPEs enable the transformation of approximately 60–80% of free water into bound water [29,30]. This transition significantly: (1) reduces water activity and increases HER overpotential;

(2) promotes Zn^{2+} desolvation; (3) constructs continuous ion transport channels to enhance ionic conductivity; and (4) suppresses side reactions, thereby improving Coulombic efficiency. In addition, HPEs possess considerable mechanical strength, enabling the formation of a compressive stress barrier at the electrode interface to block dendrite growth. Their lightweight nature, compact volume, and inherent deformability also make them attractive candidates for next-generation flexible and wearable electronics [31–33]. In summary, HPEs provide a highly promising platform for high-performance, long-lifespan and safe aqueous ZIBs. This potential arises from a combination of their "solid–liquid synergistic mechanism" (which integrates the mechanical robustness of solid electrolytes with the high ionic conductivity of liquids), the water confinement effect (which reduces water activity and suppressed undesirable side reactions), and the presence of abundant functional groups (which promote uniform Zn deposition and inhibit dendrite growth) [34,35].

This review provides a comprehensive summary of recent advances in HPEs, including their material composition, structural evolution, ion transport mechanisms, and electrochemical performance. It also discusses the fundamental energy storage mechanisms of ZIBs and the commonly used electrode/electrolyte materials to offer a holistic understanding of the HPE-ZIB interface. The goal is to provide insight into the current status, unresolved challenges, and future prospects of HPE-integrated aqueous ZIBs.

2. Overview of ZIBs

ZIBs, as an important class of electrochemical energy storage devices, typically comprise a cathode, an anode, and an electrolyte that bridges the two electrodes. In ZIB systems, metallic zinc (Zn) is commonly employed as the anode, while HPEs have become the focal point of recent research. The electrolyte plays a pivotal role in battery operation, serving three primary functions: (1) constructing ion transport channels to enable the efficient migration of charge carriers (e.g., Zn^{2+}) between the cathode and anode; (2) maintaining charge balance within the system; and (3) regulating the interfacial reaction kinetics at the electrode surfaces. Together, these functions are essential for ensuring efficient charge transfer and the smooth operation of energy storage and release processes.

2.1. Energy Storage Mechanisms of Aqueous ZIBs

ZIBs exhibit a wide variety of charge storage mechanisms. The main mechanisms proposed to date include: (1) Zn^{2+} insertion/extraction; (2) proton (H^+)-Zn^{2+} co-insertion; (3) chemical phase transformation pathway; (4) coordination-driven conversion reactions; (5) hybrid-ion migration; and (6) anion intercalation/deintercalation processes [36]. The following section elaborates on the first three representative mechanisms.

Zn^{2+} insertion/extraction. This process, analogous to that in LIBs, involves the reversible insertion and extraction of Zn^{2+} within the cathode host lattice [37,38]. During discharge, Zn^{2+} migrates from the anode to the cathode and inserts into its lattice, accompanied by the reduction in the cathode material (electron acceptance). During charging, the reverse occurs: Zn^{2+} is extracted from the cathode, redeposited onto the anode, and the cathode material undergoes oxidation. To maintain charge balance, the metallic Zn anode simultaneous experiences dissolution (stripping) and deposition during cycles. Taking the aqueous Zn/δ-MnO_2 battery as an example, although it has attracted significant attention for its cost-effectiveness, safety, and environmental compatibility, its precise charge storage mechanism remains under debate [39]. While Zn^{2+} insertion/extraction is widely accepted, recent studies suggest possible H^+ co-insertion or phase transformation during cycling, complicating the understanding of capacity decay [40]. Cui et al. [41] revealed for the first time that Zn^{2+} irreversibly embeds into the δ-MnO_2 structure mainly through an ion-exchange process prior to electrochemical cycling (Figure 1a), rather than

through electrochemical insertion itself. This ion-exchange-mediated pre-intercalation contributes minimally to the electrode's capacity during cycling. Their work further demonstrated that the charge storage process of the δ-MnO_2 electrode is primarily governed by electrochemical H^+ insertion/extraction, electrochemical dissolution of δ-MnO_2, and the electro-dissolution/electrodeposition behavior of vermiculite. This finding provides new fundamental insights into the reaction mechanisms of δ-MnO_2 electrodes in aqueous batteries.

H^+-Zn^{2+} co-insertion behavior. In aqueous environments, the divalent nature and large hydrated radius of Zn^{2+}, typically present as $[Zn(H_2O)_6]^{2+}$, impose significant constraints on its transport within electrode materials. These constraints manifest in two primary ways: (1) the high charge density of Zn^{2+} induces strong Coulombic repulsion, causing substantial lattice strain during ion insertion; and (2) the extensive hydration shell increases the effective ionic radius, thereby elevating the activation energy for migration through the host lattice. These factors severely impede electrode reaction kinetics and compromise structural stability, ultimately leading to rapid capacity degradation and electrode corrosion, particularly under high-rate charge/discharge conditions [42,43]. To mitigate these issues, incorporating small, low-valence auxiliary ions such as H^+ has emerged as an effective strategy to enhance electrochemical performance [44,45]. Protons exhibit high mobility and readily participate in electrochemical reactions. Their lower charge density minimizes electrostatic repulsion and facilitates rapid diffusion and distribution through the host matrix. Crucially, the fast diffusion and uniform distribution of H^+ ions enable more efficient access to active sites within the electrode structure, thereby improving energy density, power density, and cycling stability. For instance, Sun et al. [46] first elucidated the electrochemical mechanism of H^+/Zn^{2+} co-insertion in a Zn/MnO_2 aqueous battery system (Figure 1b). Using the galvanostatic intermittent titration technique (GITT), they identified two distinct kinetic regions (Region I and Region II) during discharge, characterized by markedly different polarization behavior. In Region I, a polarization voltage of only 0.08 V was observed, significantly lower than the 0.6 V in Region II. This indicated lower ohmic and charge-transfer resistances in Region I, where H^+ insertion dominates. Moreover, the diffusion coefficient of H^+ was found to be two orders of magnitude higher than that of Zn^{2+} in Region II. These results strongly support a dual-stage energy storage mechanism: preferential H^+ insertion in the early stage (Region I), followed by Zn^{2+}-dominated insertion in the latter stage (Region II). This dual-ion transport model provides critical insights into the complex energy storage mechanisms of aqueous ZIBs.

Chemical phase transformation Pathway. For certain cathode materials, the energy storage mechanism is governed not by classical ion intercalation but by reversible chemical conversion reactions. Zhang et al. [47] developed a novel SnS_2@C composite via a facile hydrothermal process and employed it as a cathode material in ZIBs (Figure 1c–e). The incorporation of conductive carbon nanosheets significantly improved the microstructure of SnS_2, increasing the exposure of electrochemically active sites and accelerating both ion and electron transport kinetics. As a result, the optimized SnS_2@C-1.6 cathode delivered a specific capacity of 136.2 mAh g^{-1} at a current density of 5 A g^{-1}, with negligible capacity decay over 2300 cycles, even at an ultra-high current density of 20 A g^{-1}. Comprehensive ex situ characterizations demonstrated that the Zn^{2+} storage mechanism in the SnS_2@C-1.6 cathode was dominated by the reversible adsorption of Zn^{2+} on the (101) crystalline facet of SnS_2, along with a chemical phase transformation in which SnS_2 was converted into ZnS and metallic Sn during discharge, with the reverse reaction occurring during charge. This work not only provides a valuable design strategy for cathode developing in ZIBs but also broadens the current understanding of alternative electrochemical energy storage pathways beyond intercalation chemistry.

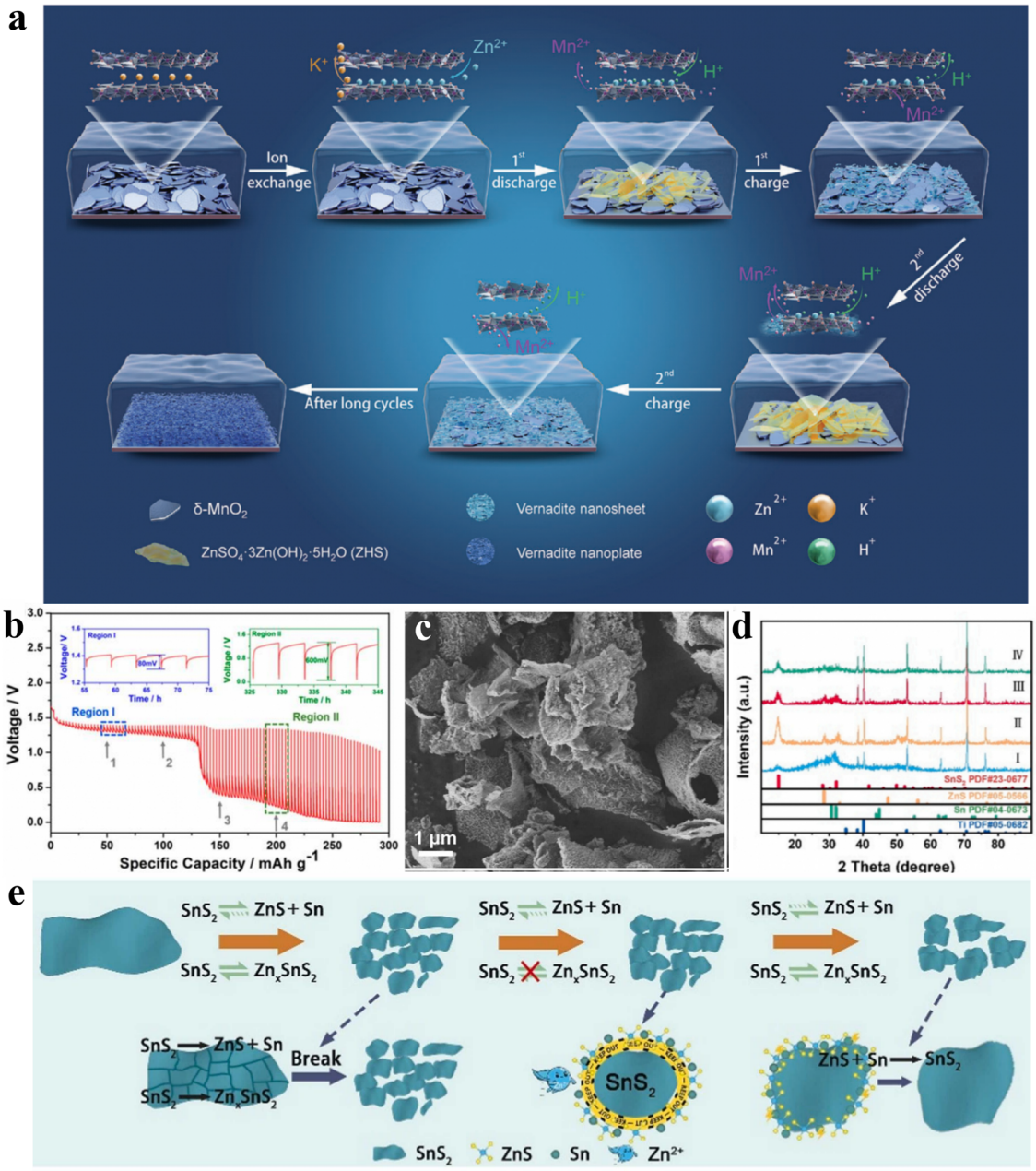

Figure 1. Charge storage mechanisms of ZIBs. (**a**) Illustration of the reaction process of δ-MnO_2 electrode in aqueous ZIBs [41]. (**b**) GITT profiles of the Zn/MnO_2@CFP cell [46]. (**c**) SEM images of SnS_2@C−1.6 [47]. (**d**) Ex situ XRD patterns of SnS_2@C−1.6 [47]. (**e**) Schematic diagram of the competition-cooperation mechanism of the SnS_2@C−1.6 cathode during cycling (The dashed arrow illustrates the dynamic process of structural evolution in SnS_2 nanosheets across various electrochemical cycling stages.) [47].

2.2. *Anode Materials for Aqueous ZIBs*

Metallic zinc (Zn) is one of the most widely used anode materials in aqueous ZIBs and other Zn-based energy storage systems, such as zinc-air and zinc-nickel batteries [48,49]. Compared to alkali metals like lithium, sodium, and potassium, Zn offers superior thermodynamic stability in aqueous environments. It is less prone to severe side reactions and presents no risk of combustion or explosion, making it an intrinsically safer and more stable anode choice for ZIBs. Despite these advantages, practical implementation of Zn anodes is hindered by several critical challenges, primarily uncontrollable dendrite growth,

which results in poor reversibility and low Coulombic efficiency, ultimately compromising large-scale deployment [50,51].

In alkaline electrolytes, Zn anodes suffer from pronounced dissolution coupled with the hydrogen evolution reaction (HER), leading to the formation of supersaturated zincate ions ($[Zn(OH)_4]^{2-}$). When the local concentration of $[Zn(OH)_4]^{2-}$ exceeds the solubility limit, insoluble byproducts such as ZnO or $Zn(OH)_2$ precipitate and accumulate on the electrode surface, causing anode passivation [52]. These deposits not only reduce the reversibility and utilization rate of Zn, but also accelerate capacity fading and Coulombic efficiency degradation during long-term cycling. Moreover, the passivated surface fails to prevent Zn dendrite growth; its inherent structural inhomogeneity can even exacerbate dendrite formation, increasing the risk of internal short circuits.

In neutral or mildly acidic electrolytes such as $Zn(CF_3SO_3)_2$ and $ZnSO_4$ aqueous solutions, side reactions are somewhat mitigated, but dendrite formation remains a persistent issue, especially under high current densities or with high cathode mass loading. Furthermore, HER and corrosion reactions still occur in these environments, leading to continuous consumption of Zn metal and electrolyte, deterioration in Coulombic efficiency, and poor long-term cycling stability [53].

Therefore, the development of advanced electrolyte systems, particularly HPEs, has become imperative. Bu suppressing Zn dendrite growth and mitigating interfacial side reactions (e.g., HER and corrosion), HPEs offer a promising strategy to enhance Zn anode stability and extend the overall cycle life of aqueous ZIBs.

2.3. Cathode Materials for Aqueous ZIBs

Cathode materials for aqueous ZIBs can be broadly classified into five primary categories: manganese oxides and their derivatives, transition metal ferricyanides (Prussian blue analogs, PBAs), vanadium-based compounds, organic electrode materials, and lithium-doped or composite materials.

Manganese oxides and derivatives. Manganese-based compounds have attracted extensive attention in ZIB cathode due to their relatively high redox potential (enabling higher operating voltage plateaus), abundant raw material reserves, low cost, and well-established synthesis techniques [54]. Recent advancements have significantly improved their specific capacity and cycling stability, highlighting their potential for large-scale application. The rich valence states of manganese (Mn^{2+}, Mn^{3+}, Mn^{4+}, Mn^{7+}) endows its oxides with unique electrochemical properties [55]. These materials adopt diverse crystallographic structures (as illustrated in Figure 2a), including tunnel types (α, β, γ), layered types (δ), and spinel types (λ) frameworks [56–60], some of which are highly conducive to reversible Zn^{2+} insertion/extraction [57–60]. However, manganese dissolution during repeated cycling remains a critical issue, leading to active material loss and shortened battery lifespan [61].

Vanadium-based compounds. Vanadium-based oxides such as V_2O_5, VO_2 and V_6O_{13}, feature diverse vanadium–oxygen coordination geometries (e.g., tetrahedral, square pyramidal, trigonal bipyramidal, octahedral) and variable oxidation states (V^{3+}, V^{4+}, V^{5+}), conferring versatile electrochemical behavior. These materials typically form chain-like or layered frameworks via edge- or corner-sharing of VO_x polyhedra (Figure 2b), with intercalated anions (e.g., Cl^-, $SO_4{}^{2-}$) to balance charges and stabilize the structure [62–64]. For instance, Dai et al. [65] designed a freestanding reduced graphene oxide (RGO)/VO_2 composite film cathode, which exhibited excellent cycling stability, with a high reversible specific capacity of 240 mAh g^{-1} and remarkable retention after 1000 cycles at 4 A g^{-1}. The assembled cell delivered an energy density of 65 Wh kg^{-1} at a power density of 7.8 kW kg^{-1}. The composite film provided effective channels for electron and ion transport and mitigated volume expansion induced by Zn^{2+} insertion. Furthermore, doping

strategies have been shown to effectively tailor the electronic structure of VO_2(B), thereby enhancing reaction kinetics.

Transition metal ferricyanides (PBAs). PBAs, as a class of open-framework transition metal cyanides, have emerged as promising ZIB cathodes due to their unique crystal structure and favorable electrochemical characteristics [66–68]. Their cubic lattice (Figure 2c) comprises alternating [FeC_6] and [MN_6] octahedra, where Fe^{3+} and transition metals (e.g., Zn^{2+}, Cu^{2+}, Mn^{2+}, Fe^{2+}) coordinate with carbon and nitrogen atoms, respectively, creating 3D channels ideal for the reversible insertion of hydrated Zn^{2+} ions. ()Since the first report of a zinc hexacyanoferrate (ZnHCF) cathode in 2014, PBAs have achieved high operating voltage plateau (~1.7 V), although early versions exhibited limited specific capacities (<100 mAh g^{-1}) [69]. Recent research has focused on optimizing transition-metal sites, engineering vacancy defects, and forming composite structures, significantly enhancing specific capacity (up to 160 mAh g^{-1}) and cycling stability (> 90% capacity retention after 2000 cycles), providing a new direction for developing high-voltage, long-life ZIBs.

Organic electrode materials. Since the 1970s, organic compounds with quinone-based redox groups have been explored for rechargeable batteries [70]. Quinone derivatives, such as benzoquinone, anthraquinone, and naphthoquinone, are valued for their redox properties [71]. Their molecular skeletons, rich in multi-carbonyl functional groups (redox-active centers) and extended π-conjugated electron systems, enable theoretical specific capacities of up to 300 mAh g^{-1}. Importantly, they exhibit exceptional chemical inertness and structural robustness in aqueous electrolytes [72], showing minimal dissolution under acidic or neutral condition. This high electrochemical stability mitigates active material loss during cycling, thereby enhancing the long-term performance and electrode lifespan. Collectively, these features make organic electrode materials highly promising for aqueous metal-ion batteries, particularly ZIBs, where interfacial stability and electrolyte compatibility are critical.

Lithium-doped/composite materials. Some well-established LIB cathode materials, after appropriate modified, have been repurposed for aqueous ZIBs. Among these, spinel-type $LiMn_2O_4$ has attracted attention due to its 3D lithium-ion diffusion channels, offering advantages of low cost, good rate performance, and high thermal stability. However, its relatively low specific energy density and capacity fading during prolonged cycling remain limitations. To address these issues, strategies such as lattice doping to stabilize the crystal structure, surface coating to inhibit interfacial side reactions, and constructing composites to enhance electrical conductivity and structural integrity have been employed. For example, Wu et al. [73] synthesized an octahedral $LiMn_2O_4$ composite with oxygen vacancies, donated as TiO_2@(LMO-A0.5), which retained 91.22% of its initial capacity after 200 cycles at 0.1 A g^{-1}, with a reversible capacity of 85 mAh g^{-1}. Similarly, olivine-type lithium iron phosphate ($LiFePO_4$), noted for its robust crystal structure, environmental friendliness, and cost-effectiveness, has been investigated for ZIBs. Its rigid framework tolerates the lattice stress caused by Zn^{2+} intercalation. Ye et al. [74] reported an aqueous ZIB using a $LiFePO_4$ cathode, achieving high Coulombic efficiency (~100%), excellent cycling stability (92 mAh g^{-1} after 400 cycles at 6C rate) and strong rate capability (72 mAh g^{-1} at 3C; 45 mAh g^{-1} at 6C), with an average working voltage of 1.2 V. Carbon-coated $LiFePO_4$ cathodes further enhance electrochemical stability, typically exhibiting a discharge plateau of ~1.2 V and a reversible capacity of ~120 mAh g^{-1}, with <10% capacity loss after 500 cycles. These results highlight the potential of lithium-based composite cathodes as low-cost, high-safety alternatives for future zinc-based energy storage systems.

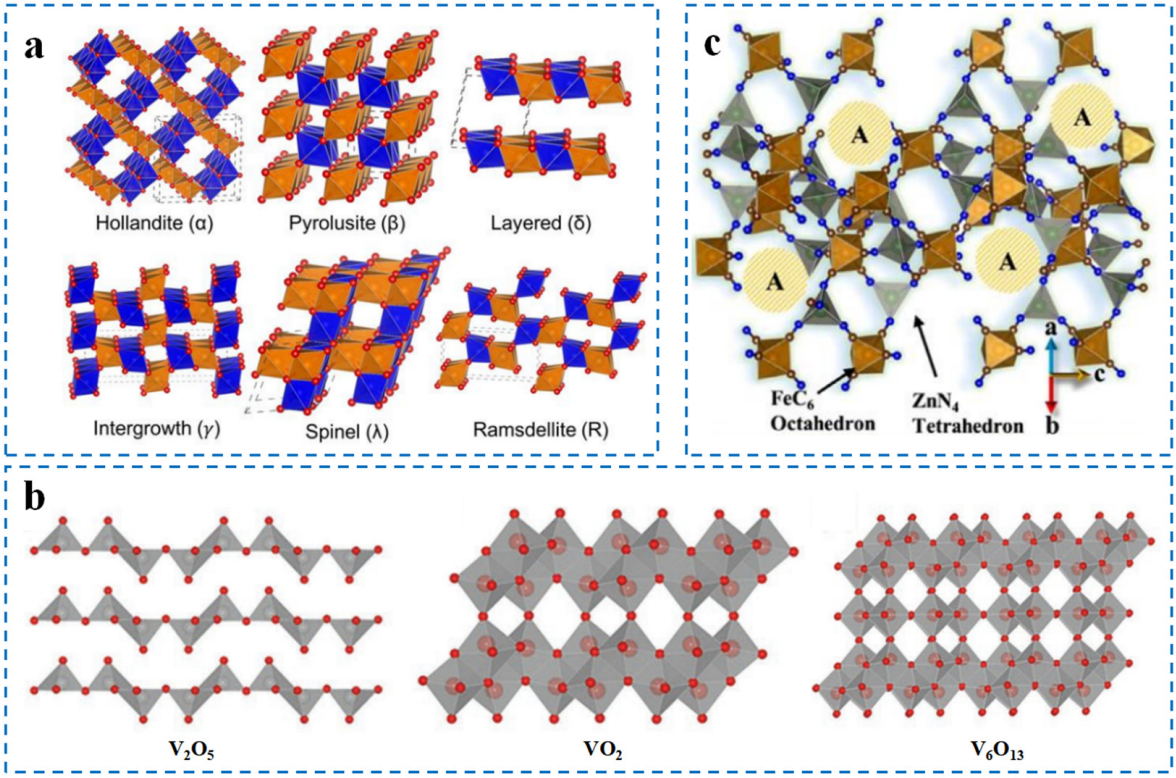

Figure 2. Crystal structures of common cathode materials for ZIBs. (**a**) MnO_2 [56]. (**b**) Vanadium-Based Compounds [64]. (**c**) ZnHCF (A denotes the cavities in the crystal structure) [68].

2.4. Electrolytes for Aqueous ZIBs

Electrolytes play a critical role in determining the performance, stability, and safety of aqueous ZIBs. Among various options, aqueous electrolytes have attracted sustained attention owing to their inherent advantages, including environmental friendliness, low cost, and high ionic conductivity. Historically, early ZIB systems primarily employed strongly alkaline electrolytes, such as LiOH, NaOH, or KOH solutions, reflecting their successful use in conventional Zn-based energy storage devices like Zn/MnO_2 primary batteries, Zn/Ni secondary batteries, and Zn/Ag batteries [75]. Among them, KOH-based electrolyte were particularly favored due to their highly alkaline environment, which enhances Zn salt solubility and enables rapid ion transport, resulting in low ohmic resistance and fast interfacial reaction kinetics [76]. However, alkaline systems suffer from several inherent limitations in rechargeable ZIBs: (1) low Zn anode deposition/stripping efficiencies (typically < 85%); (2) uncontrollable Zn dendrite growth during cycling; and (3) persistent byproduct formation (e.g., ZnO or $Zn(OH)_2$), leading to electrode passivation, increased interfacial impedance, capacity degradation, and Coulombic efficiency below 90%. These shortcomings have driven the transition towards neutral to mildly acidic electrolytes, such as $ZnSO_4$ and $Zn(CF_3SO_3)_2$, which offer improved interface compatibility and electrochemical reversibility.

In ZIBs, the interfacial stability between the Zn electrode and electrolyte is crucial to long-term cycling performance [77]. In alkaline electrolytes, the abundance of OH^- ions induce intense Zn corrosion and rapid formation of $ZnO/Zn(OH)_2$, greatly compromising the anode surface and reducing battery life [78]. In contrast, mildly acidic electrolytes, which contain trace amount of H^+, can suppress interfacial side reactions while retaining adequate ionic conductivity, thereby improving anode stability [79].

Despite these improvement, aqueous ZIBs continue to face critical challenges, such as persistent corrosion, dendrite growth and capacity fade, particularly from the dissolution

of cathode active materials (e.g., Mn- and V-based compounds) in mildly acidic media [80]. Electrolyte composition engineering, especially via functional additives, has emerged as an effective approach to regulate interfacial chemistry and enhance electrochemical performance [81,82]. For example, in Mn-based cathodes, adding a moderate concentration of $MnSO_4$ establishes a dynamic dissolution-deposition equilibrium [83]. This equilibrium maintains the Mn^{2+} concentration at an optimal level, promoting the formation of a protective deposition layer (e.g., MnO_2 or Mn_3O_4) on the cathode. The layer acts as a selective Mn^{2+} capture interface, effectively suppressing continuous dissolution of active material and significantly enhancing structural integrity and cycling stability [84]. This approach has been extended to other systems, including V-based and Co-based ZIBs, demonstrating broad applicability [85]. Furthermore, introducing Na^+ ions into $ZnSO_4$ electrolytes yields synergistic benefits. Besides stabilizing the cathode through competitive equilibrium, Na^+ ions preferentially adsorb on the electrode surface during Zn plating, forming a positive electrostatic shield that modulates local electric fields and inhibits dendritic nucleation and growth [86]. These multi-scale synergistic effects represent a forward-looking design paradigm for next-generation, high-performance aqueous ZIB electrolytes.

Beyond the conventional aqueous electrolytes (including alkaline, neutral, and mildly acidic) discussed above, several advanced strategies have been developed to enhance the performance of ZIBs, among which water-in-salt electrolytes (WISEs) and ionic liquid (IL)-based electrolytes have attracted considerable attention. WISEs are formed by dissolving extremely high concentrations of salts (e.g., $Zn(TFSI)_2$, $ZnCl_2$) in water, which markedly reduces the number of free water molecules and reconstructs the Zn^{2+} solvation structure [87,88]. This effectively suppresses side reactions such as hydrogen evolution and electrode dissolution, while also inhibiting dendrite formation. Furthermore, WISEs significantly broaden the electrochemical stability window, enabling the integration of high energy density with intrinsic safety. However, their ultrahigh salt concentration inevitably leads to substantially increased cost and elevated viscosity, leading to lower ionic conductivity and compromised rate capacity [89]. Similarly, IL-based electrolytes offer advantages such as non-flammability, low volatility, and a wide electrochemical window. Nevertheless, the high synthesis cost, inherent high viscosity, limited ionic conductivity and unsatisfactory interfacial compatibility with electrodes pose significant challenges for their practical application [90,91]. Therefore, despite their promise for constructing safer and higher-energy-density ZIBs, the inherent limitations of WISEs and IL-based electrolytes hinder their widespread adoption.

In this context, HPEs have emerged as a highly promising alternative by offering a unique balance of favorable properties. HPEs retain the high ionic conductivity and cost-effectiveness of traditional aqueous electrolytes, while incorporating a three-dimensional cross-linked polymer network that confines free water molecules and reduces water activity, thereby effectively suppressing water-related side reactions such as HER and corrosion [92,93]. Moreover, the functional groups within the polymer matrix can regulate Zn^{2+} solvation/desolvation behavior through ion-polymer coordination, promoting uniform Zn deposition. The mechanical robustness and elasticity of HPEs additionally provide physical resistance against dendrite growth and maintain structural integrity under repeated deformation, making them particularly attractive for flexible and wearable ZIBs [19,93,94]. Collectively, these features highlight HPEs as a versatile and scalable electrolyte strategy to address the intrinsic challenges of liquid electrolytes, thereby paving the way for developing safe, durable, and high-performance aqueous ZIBs.

3. Research Progress on HPEs in Aqueous ZIBs

HPEs, a class of solid or semi-solid electrolytes formed through physical or chemical cross-linking, possess a 3D network architecture that combines solid–liquid hybrid characteristics. HPEs feature a porous framework constructed by a polymer matrix, which serves a dual function. On one hand, the polymer skeleton confines both free and bound water molecules via intermolecular interactions, such as hydrogen bonding and van der Waals forces, thereby preserving the mechanical integrity of the hydrogel even under humid or aqueous conditions. On the other hand, the water retained within the network pores forms a dynamic hydration layer, enabling self-regulated swelling behavior. This structure design allows HPEs to simultaneously exhibit the high ionic conductivity of liquid electrolytes (typically 10^{-2} to 10^{-1} S cm^{-1}) and the mechanical resilience of solid-state systems. Importantly, the degree of swelling, and thus ionic mobility, can be tuned by adjusting the cross-linking density, providing aqueous ZIBs with a safe and electrochemically active electrolyte system characteristic of quasi-solid-state electrolytes [95]. Additionally, HPEs generally possess a high Zn^{2+} transference number, which mitigates concentration polarization and improves electrochemical performance. Beyond electrochemical advantages, HPEs offer favorable mechanical and interfacial properties. Their flexibility, light weight, and mechanical robustness enable excellent conformability at the electrode–electrolyte interface. At the microscopic level, the nanoscale porosity of the 3D network provides a well-dispersed medium for electrolyte salts, facilitating continuous ion transport through dynamic coordination with functional groups on the polymer chains and via polymer segmental relaxation.

Despite these multifunctional attributes, several critical challenges hinder the practical deployment of HPEs in real-world ZIBs. Key issues include long-term operational stability in flexible devices, interfacial compatibility with various electrode materials, and scalability and reproducibility of fabrication processes. To date, the most widely studied HPE systems in aqueous ZIB research are based on polyacrylamide (PAM) [96,97], polyvinyl alcohol (PVA) [98], polyacrylic acid (PAA) [99], and biomass-based hydrogels [100]. In the following sections, we provide a critical review of recent advancements in the first three major categories of synthetic HPE materials.

3.1. PAM-Based Hydrogel Electrolytes

PAM, with molecular chains rich in hydrophilic amide groups (-$CONH_2$) and side-chain structures amenable to chemical functionalization, serves as a key polymer matrix for hydrogel electrolytes in flexible ZIBs. Its 3D network can be formed via hydrogen bonding and covalent cross-linking, endowing PAM hydrogels with high water absorption and retention (water content > 90%), environmental friendliness, and excellent interfacial adhesion to Zn electrodes (adhesion strength exceeding 30 kPa). The advantages of PAM-based hydrogels in flexible ZIBs primarily lie in mechanical adaptability and interfacial stability. The hydrophilic -$CONH_2$ groups facilitate strong hydrogen bonding at the electrode–electrolyte interface, effectively reducing interfacial slippage during cycling. Meanwhile, the flexible PAM backbone provides excellent stretchability, with tensile strains exceeding 500% in some cases [101]. Additionally, polar functional groups (e.g., C=O) on the polymer chains can guide uniform Zn deposition along the (002) crystal plane, enabling Zn | | Zn symmetric cells to achieve a lifespan exceeding 1800 h [102]. Beyond mechanical robustness, PAM-based hydrogels can regulate the Zn^{2+} solvation structure via coordinating with polar functional groups, reducing the activity of free water. This suppresses parasitic HER and corrosion while promoting uniform zinc deposition [102]. These features collectively enhance both electrochemical performance and interface stability.

Despite these advantages, PAM hydrogels still face limitations that constrain their practical applications. Their intrinsic mechanical strength is typically below 200 kPa, making them prone to structural collapse under compressive stress. Additionally, their ionic conductivity (typically 3.5–33.8 mS cm^{-1}) can decrease significantly at low temperatures due to restricted chain segment mobility. Furthermore, covalently cross-linked PAM networks are difficult to dissociate, limiting environmental compatibility and self-healing capabilities [103]. These deficiencies lead to two critical issues: a sharp decline in ion transport efficiency under high current densities or extreme conditions, and performance degradation caused by electrode–electrolyte contact failure after mechanical damage.

To address these challenges, recent studies have developed innovative design strategies based on multiscale structural engineering and synergistic functional integration. For example, Shen et al. designed a highly entangled HE-PAM hydrogel (Figure 3a) [104]. By extending polymer chains to form a dense interpenetrating network, the elastic modulus increased nearly 10-fold while simultaneously lowering the ion migration energy barrier. For full-cell validation, the Zn||MnO_2 pouch cell employing HE-PAM as the electrolyte was systematically evaluated. The areal loading of the cathode was determined to be over 5 mg cm^{-2}, satisfying the practical applications requirement. Electrochemically, the cell exhibited outstanding fast-charging capability and cycling stability, remaining operational even at a high current density of 35 A g^{-1}, indicative of superior rate performance. After 2000 cycles at 10 A g^{-1}, the capacity retention remained as high as 80.05%, demonstrating excellent long-term cycling durability.

Inspired by plant stems, Wen's team developed a "chain-gear" topological network (Figure 3b), in which polymer micelles acted as "gears" supporting polyanion chains to form hierarchical porous channels [105]. This architecture simultaneously enhanced multiple properties, achieving an ionic conductivity of 60.6 mS cm^{-1} (measured by electrochemical impedance spectroscopy (EIS) at room temperature using a hydrogel electrolyte soaked in 2 M $ZnSO_4$ + 0.2 M $MnSO_4$ solution), a Zn^{2+} transference number of 0.88 (determined by the Bruce-Vincent method under a 10 mV DC bias in a Zn||Zn symmetric cell at room temperature), and a remarkable compressive strength of 11.3 MPa. Similarly, Zeng et al. constructed a self-healing double-network hydrogel (PAM-PAAS-QCS) incorporating Schiff base linkages, achieving room-temperature self-healing, ultrahigh stretchability (>5100%), and high ionic conductivity (33.61 mS cm^{-1}) [106]. Biomimetic strategies employed trehalose as a network repair agent (Figure 3c) strengthened hydrogen bonds, elevating tensile strength to 100 kPa and extending fracture elongation to 5338% [101]. In dynamic cross-linking, reversible borate ester bonds and hydrogen bonds endowed double-network hydrogels with self-healing capabilities, enabling damaged batteries to maintain capacities >103 mAh g^{-1} [107]. These advances demonstrate that reducing free water activity (water content ≈ 60%) via water-lean designs, combined with interfacial chemical stability, can synergistically improve mechanical robustness, ion transport, and environmental adaptability. Such strategies pave the way for practical application of flexible ZIBs.

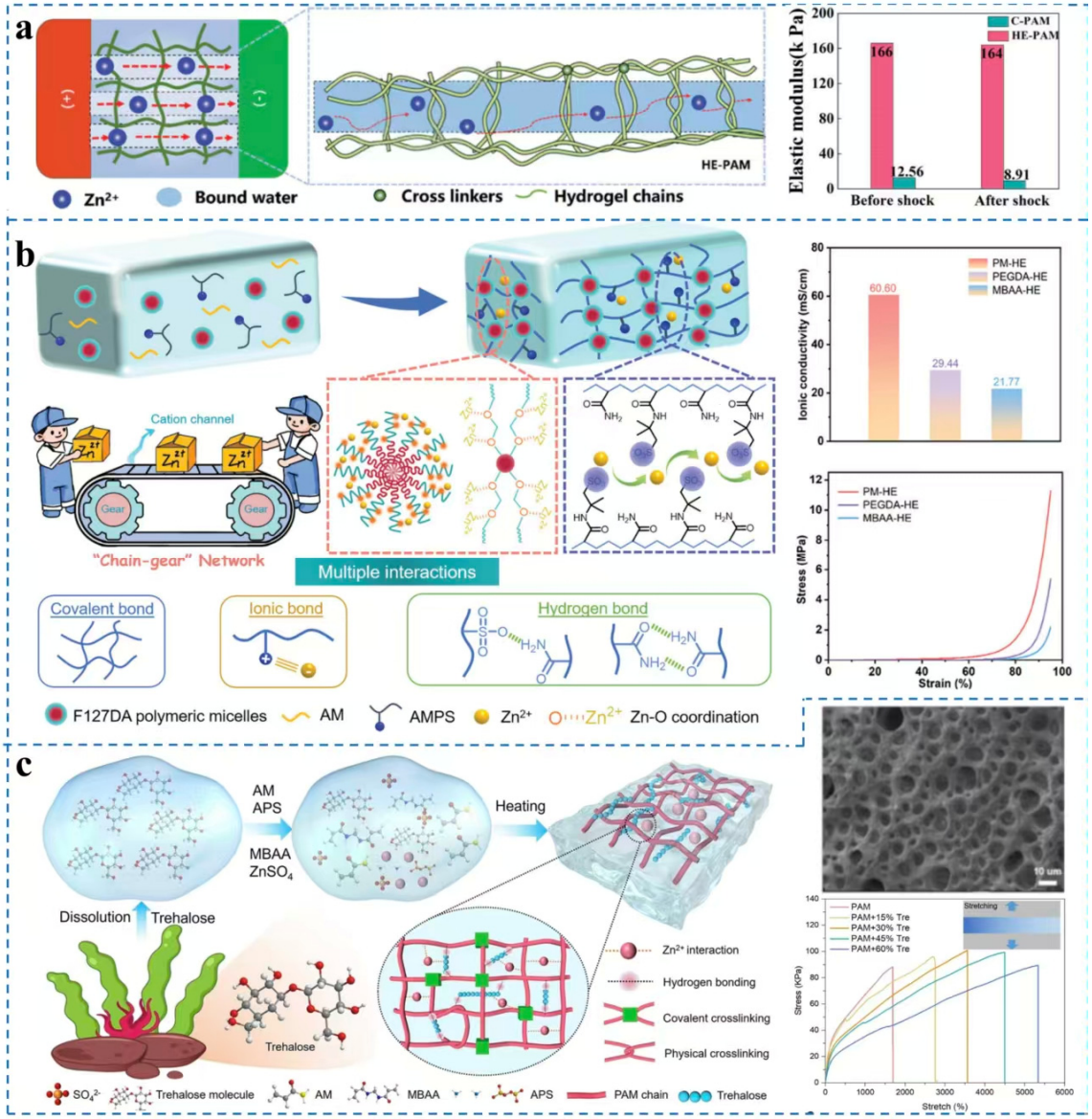

Figure 3. Representative structural and functional enhancements of PAM-based hydrogels. (**a**) Internal microstructure and elastic modulus of HE-PAM hydrogel electrolyte (Red arrows represent the migration pathway of Zn^{2+} ions through the hydrogel network) [104]. (**b**) Schematic illustration of the synthesis of the "chain-gear" hydrogel electrolyte and its mechanical property [105]. (**c**) Schematic illustration of the fabrication process for thehalose-modified PAM hydrogel and its SEM image and tensile stress–strain curves [101].

3.2. Polyvinyl Alcohol (PVA)

PVA, with a high density of hydroxyl groups along its molecular chains, readily forms a 3D network structure via hydrogen bonding. This structural feature endows PVA-based hydrogels with excellent water retention capacity (typically > 80 wt%) and notable mechanical strength, with modulus values reaching the megapascal level. The interplay between the crystalline and amorphous regions provides a favorable balance between flexibility and structural integrity, while ensuring long-term dimensional stability in aqueous environments. These combined properties make PVA an attractive matrix for hydrogel electrolytes in flexible aqueous ZIBs [103]. However, conventional PVA hydrogels still suffer from several inherent limitations, including relatively low ionic conductivity

(usually < 20 mS cm^{-1}), poor recyclability, and susceptibility to freezing under sub-zero conditions, all of which hinder their practical applications.

To overcome these challenges, researchers have explored strategies focusing on cross-linking optimization, structural engineering design, and functional composite incorporation. For instance, dynamic borate cross-linking was employed by Cao et al. to develop the P3B2Zx hydrogel (Figure 4a) [108]. Borate ester bond recombination and dehydration-induced chain entanglement formed continuous ion channels, enabling Zn||Zn batteries to operate stably for over 1500 h at −20 °C while offering excellent recyclability. Similarly, Chen's group introduced a synergistic borax/glycerol cross-linking system, reducing the freezing point to −60 °C and maintaining ionic conductivity of 10.1 mS cm^{-1} at −35 °C [109]. A flexible quasi-solid-state ZIB was fabricated by coupling this electrolyte with an rGO/MnO_2 cathode (active mass loading ≈4 mg cm^{-2}) and a zinc foil anode. The device delivered a high energy density of 46.8 mW h cm^{-3} (1330 μW h cm^{-2}) and a power density of 96 mW cm^{-2} (2.7 mW cm^{-2}) at 25 °C. Remarkably, even under an extreme low temperature of –35 °C, the battery retained an energy density of 25.8 mW h cm^{-3} (approximately 55% of the room-temperature value) and exhibited outstanding cycling stability, maintaining about 90% capacity retention after 2000 cycles.

Beyond chemical modifications, structural engineering has proven effective for performance enhancement. Wang et al. constructed a gradient-networked hydrogel electrolyte (PCG20-PC5) inspired by the layered structure of articular cartilage. The cathode-facing layer was composed of low-network-density PVA/cellulose nanofiber (PVA/CNF, PC) hydrogel, featuring large pores (15–40 μm) and high water content, which significantly promoted ion transport. Conversely, the anode-facing layer was a high-network-density PVA/CNF/graphene oxide (PCG) hydrogel with smaller pores (3–6 μm) and abundant carboxyl and hydroxyl groups, which facilitated Zn^{2+} desolvation, reduced water activity, and homogenized ion flux (Figure 4b). The introduction of graphene oxide (GO) further augments the dielectric properties and electronegativity of the electrolyte, resulting in an increased Zn^{2+} transference number (0.45) and high ionic conductivity (16.18 mS cm^{-1}). This gradient structure not only optimizes interfacial chemistry but also synergistically enhances the uniformity of zinc deposition and reaction kinetics. As a result, the Zn||Zn symmetric cell based on this electrolyte exhibits exceptional cycling stability for over 2200 h at 1 mA cm^{-2}. The corresponding Zn-MnO_2 full cell demonstrates superior rate capability over 0.15–3 A g^{-1} and an ultralow capacity decay rate of 0.013% per cycle after 800 cycles, indicating outstanding cycling stability and interfacial compatibility [110]. Wu et al. designed a hierarchical porous structure within a pullulan-reinforced double-network hydrogel (PPZ), using interchain hydrogen bonding to stabilize the network. This system supported symmetric cells cycling for 400 h without performance degradation at a depth of discharge (DOD) of 17.08% [111]. Du et al. introduced PVA-borax hydrogel as an interfacial layer at zinc anode, homogenizing the local electric field but also reducing the corrosion current density to 0.029 mA cm^{-2}, thereby improving surface uniformity and interfacial stability [112].

Incorporating functional composites into the PVA matrix has also shown promise. Zhu et al. [113] incorporated conductive polyaniline (PANI) and nano-SiO_2 into PVA hydrogels. The amine groups of PANI homogenized charge distribution, while the hydroxyl groups of SiO_2 formed hydrogen bonds with PVA chains. This design yielded a Zn^{2+} transference number of 0.56 and an electrochemical window of 2.56 V, effectively suppressing zinc dendrites and enabling stable Zn||Zn cycling for over 1200 h with minimal polarization (0.182 V). Similarly, Long et al. combined a Prussian blue analog cathode with a PVA/PAM gel electrolyte, exploiting Co/Fe dual redox reactions to expand the working voltage window to 1.85 V, with capacity retention exceeding 83% after 3000 mechanical bending

cycles [107]. Yu et al. developed a polyanion-functionalized hydrogel (PMZA) based on 2-2-acrylamide-2-methylpropanesulfonic acid and PVA [114]. This PMZA electrolyte demonstrated an exceptional ionic conductivity of 71.17 mS cm^{-1}, as measured by EIS using a stainless steel (SS) | electrolyte | SS cell. Moreover, the electrolyte achieved an ultra-high Zn^{2+} transference number of 0.912, calculated via the Bruce-Vincent under potentiostatic polarization with a 10 mV DC bias applied to a Zn | | Zn symmetric cell. Both properties were characterized at room temperature with 2M $ZnSO_4$ as the supporting electrolyte. This efficient ion transport enabled Zn-NVO full cells to operate without capacity decay after 7000 cycles at 5 A g^{-1} (Figure 4c). Furthermore, the NVO cathode possessed an area loading of 4.5 mg cm^{-2}, underscoring the high reliability and practical applicability of the PMZA electrolyte.

Despite the significant progress in dendrite suppression, wide-temperature adaptability, and interfacial stability, the ionic conductivity of modified PVA hydrogels generally remains lower than that of liquid electrolytes. Future efforts should explore synergistic mechanisms that balance mechanical robustness with efficient ion transport. Additionally, sustainable and efficient green recycling processes, such as the "one-pot recycling method" proposed by Cao et al., [108] will be essential to advancing the commercial viability of flexible and eco-friendly zinc-ion energy storage devices.

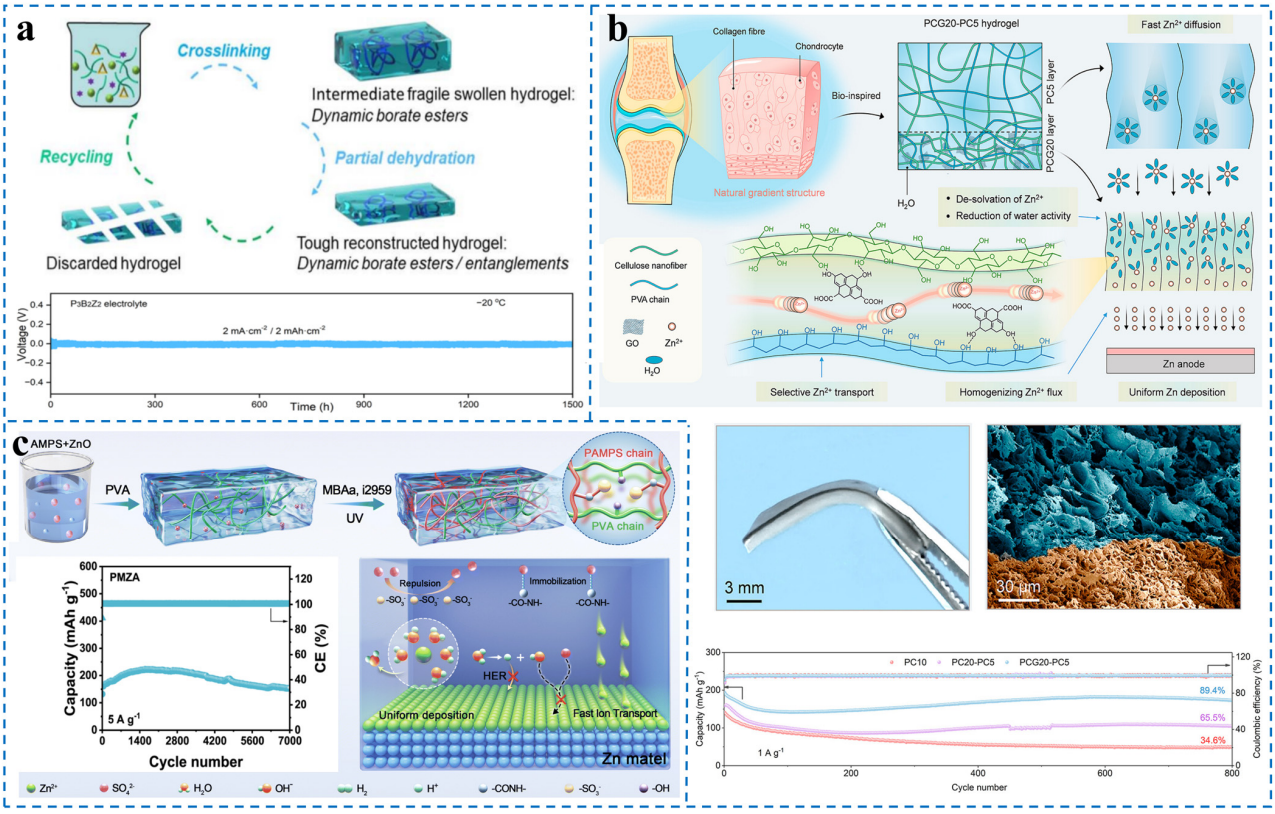

Figure 4. Representative structural and functional enhancements to PVA-based hydrogels. (**a**) Schematic illustration of the synthesis of P3B2Zx hydrogels and the Zn plating/stripping performance of a symmetric cell with the P3B2Z2 electrolyte at 2 mA cm^{-2} at −20 °C [108]. (**b**) Schematic illustration of the cartilage-inspired gradient-networked hydrogel electrolyte designed to stabilize the Zn anode, a photograph and SEM image of the as-prepared PCG20–PC5 hydrogel, and the long-term cycling performance of coin-type Zn-ion batteries employing various hydrogel electrolytes [110]. (**c**) Schematic of PMZA synthesis, hydrogel electrolyte mechanism, and Zn | PMZA | NVO full-cell cycling performance at 5 A g^{-1} [114].

3.3. Polyacrylic Acid (PAA)

PAA-based hydrogel electrolytes possess unique hydrophilicity and ion-regulation capabilities, primarily due to the regular arrangement of high-density carboxyl groups (-COOH) along their backbone. Upon ionization, these carboxyl groups form high-density negatively charged sites ($-COO^-$), contributing to construction of an extended hydration layer within the electrolyte. This structural feature enhances compatibility between the polymer network and the aqueous electrolyte. Within the 3D ion transport channels formed by PAA-based HPEs, the carboxyl groups can coordinate with Zn^{2+} ions via electrostatic interactions, effectively anchoring the charge carriers. Simultaneously, the dynamic relaxation behavior of polymer chain segments synergistically promotes ion migration, establishing an "anchoring-diffusion" dual transport mechanism. This enhances the Zn^{2+} transference number and effectively suppresses dendrite growth.

To address the inherent limitations of conventional PAA hydrogels, such as low mechanical strength (typically < 0.1 MPa) and susceptibility to freezing at low temperatures, researchers have developed multi-scale collaborative modification strategies, including chemical cross-linking reinforcement, nanocomposite enhancement, and topological structure design. For example, Chen et al. synthesized a self-healing PAA-based hydrogel by copolymerizing (3-acrylamidopropyl)trimethylammonium chloride (ATAC) in ethylene glycol (EG) [115]. The resulting dynamic hydrogen-bond network between the polycationic PATAC and the PAA/EG matrix endowed the hydrogel with intrinsic self-healing capability. When applied in zinc-air battery, the system maintained stable cycling performance even at 50 °C. Lin et al. developed a reinforced network by introducing dynamic metal-ligand coordination between Fe^{3+} ions and the carboxyl groups of a PAA/cellulose nanofibers (CNF) composite (Figure 5a) [116]. This design increased tensile strength to 44.8 kPa, provided room-temperature self-healing, and imparted strong adhesion. The modified hydrogel effectively suppressed dendrite growth, enabling Zn||Zn symmetric cells to achieve ultralong cycling stability exceeding 4600 h at −20 °C. Song et al. introduced 20 wt% Al_2O_3 nanofillers into PAA matrix. The interfacial interaction between the nanofillers and the polymer network significantly enhanced mechanical strength, increasing the tensile modulus to 104.5 kPa, which is more than that of pristine PAA hydrogel [117]. Meanwhile, the electrolyte maintained a high ionic conductivity of 186 mS cm^{-1}, as determined by EIS at room temperature. For conductivity testing, the hydrogel electrolyte was soaked in 6 M KOH + 0.2 M $Zn(AC)_2$ solution for 48 h, after which the electrolyte-saturated HPE was sandwiched between two symmetrical SS blocking electrodes) (Figure 5b). Furthermore, Xu et al. designed a double polyrotaxane (DPR) sliding-ring topological structure (Figure 5c) [118]. Stress dissipation occurs through the dynamic dissociation of reversible bonds, enabling the hydrogel to retain over 90% of its initial mechanical stress after 1000 cycles. The structure also endowed the material with room-temperature self-healing capability (63.3% efficiency after 48 h), significantly enhancing fatigue resistance.

These advancements demonstrate that rationally designed PAA-based HPEs achieve exceptional mechanical flexibility, robust interfacial compatibility, and enhanced electrochemical stability. Their synergistic capabilities in dendrite suppression, broad operating temperature window, and deformation-tolerant resilience position them as promising platforms for next-generation flexible and wearable aqueous ZIBs.

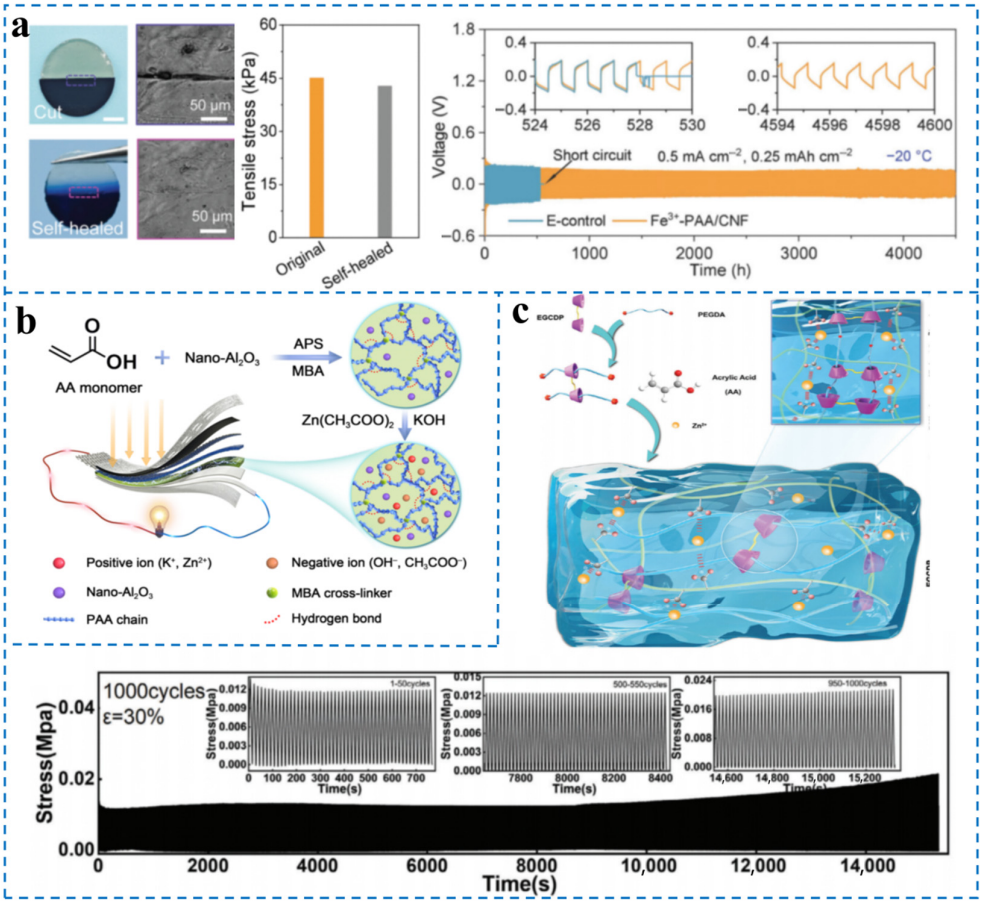

Figure 5. Representative structural and functional enhancements to PAA-based hydrogel electrolytes. (**a**) Tensile property of the Fe^{3+}-PAA/CNF hydrogel after self-healing and voltage profiles of Zn||Zn symmetrical cells at various cycling protocols (0.5 mA cm^{-2}/0.25 mAh cm^{-2}) at −30 °C. [116] (**b**) Schematic illustration of the fabrication process for the PAA-Al_2O_3 HPE and its application in the flexible zinc-air batteries [117]. (**c**) Fabrication scheme of a DPR/PAA hydrogel and its stress retention performance over 1000 continuous cyclic stretching at a fixed strain of 30% [118].

3.4. Low-Temperature Performance of HPEs

At low temperatures (−20 to −35 °C), HPEs can maintain high ionic conductivity and stable cycling performance through optimized compositional and structural design. For instance, Wei et al. developed a bond-tuned hydrogel that sustained stable cycling for over 3000 h at −20 °C with a Coulombic efficiency of 99.5%, while preserving high ionic conductivity and voltage stability in flexible pouch cells under bending conditions [119]. Ji et al. achieved 3000 h cycling of Zn||Zn symmetric cells and 600-cycle stability of full cells at −20 °C by regulating gelation behavior via compositional fluctuation, effectively balancing water activity suppression with favorable ion transport kinetics [120]. Gao et al. designed a dual-salt ($ZnCl_2$/LiCl) synergistic hydrogel electrolyte that exhibited an ionic conductivity of 7.18 mS cm^{-1} even at −70 °C [121]. Correspondingly, the Zn||PANI battery cycled 12,000 times at −70 °C and 0.5 A g^{-1} with nearly 100% capacity retention, demonstrating enhanced anti-freezing capability due to the polymer–salt eutectic effect. Additionally, Liu et al. developed a low-water-content (20%) gel electrolyte that retained a conductivity of 0.36 mS cm^{-1} at −70 °C, with symmetric cell showing stably cycling for 700 h at −40 °C, which was attributed to fast ion channels formed via proton-triggered weakly solvating polymerization [122]. These results collectively indicate that HPEs, through strategies such as high salt concentration, incorporation of zwitterionic groups, reduced water content, and multi-component synergistic design, can achieve both high

ionic conductivity and long-term cycling stability at subzero temperatures, providing a robust foundation for energy storage applications across wide temperature ranges.

Although PAM-, PVA-, and PAA-based HPEs have each achieved notable progress, they exhibit distinct structural and electrochemical characteristics that define their performance in aqueous ZIBs. PAM hydrogels offer superior stretchability and controlled Zn deposition, facilitated by abundant amide functional groups, but are susceptible to reduced ionic conductivity at low temperatures. PVA hydrogels provide notable anti-freezing capability and intrinsic self-healing due to robust hydroxyl-mediated hydrogen-bonding networks, yet ionic conductivity often remains below that of liquid electrolytes. PAA-based electrolytes feature dynamic Zn^{2+} coordination and high ionic conductivity through tailored carboxyl-group interactions, though mechanical strength can be limited in conventional designs. To provide a comparative overview, Table 1 consolidates representative mechanical properties, electrochemical performance metrics, and full-cell configurations reported in recent studies. This summary highlights the trade-offs among flexibility, conductivity, and interfacial stability, offering guidance for future design of multifunctional HPEs.

Table 1. Representative hydrogel polymer electrolytes for aqueous ZIBs reported in the literature.

Electrolyte	Tensile Strength (MPa)	Fracture Strain (%)	Ionic Conductivity (mS cm^{-1})	Zn^{2+} Transference Number	Zn||Zn Symmetric Cell (Cycle Time, Current Density/Capacity)	Full Cell Performance (Cathode||Anode, Cycles, Test Condition, Capacity Retention)	Refs.
PM-HE	0.23	790	60.6	0.88	>1500 h, 1 mA cm^{-2}/ 1 mAh cm^{-2}	Zn||MnO_2, 1000, 5 C, 91.6%	[105]
PAM/trehalose	0.1	5338	-	-	>2400 h, 1 mA cm^{-2}/ 1 mAh cm^{-2}	Zn||MnO_2, 3000, 10 A g^{-1}, 62.7%	[101]
PAM−PAAS −QCS	0.077	5100	33.61	0.72	1400 h, 0.5 mA cm^{-2}/ 0.5 mAh cm^{-2}	Zn||PANI, 1500, 1 A g^{-1}, 82.4%	[106]
PAM/PVA	0.08	1490	6.7	-	500 h, 1 mA cm^{-2}/ 1 mAh cm^{-2}	Zn||$Co_3[Fe(CN)_6]_2$, 300, 1 A g^{-1}, 79.5%	[107]
P3B2Z2	1.1	1455.6	19.4	0.53	>1500 h, 2 mA cm^{-2}/ 2 mAh cm^{-2}	Zn||KVOH, 1500, 5 A g^{-1}, 77.5%	[108]
PVA/borax/ glycerol	0.1	490	29.6	-	>1400 h, 2 mA cm^{-2}/ 2 mAh cm^{-2}	Zn||rGO/MnO_2, 2000, 1 A g^{-1}, ~90%	[109]
PCG20-PC5	0.43	320	16.18	0.45	>2200 h, 1 mA cm^{-2}/ 1 mAh cm^{-2}	Zn|| MnO_2, 800, 1 A g^{-1}, 89.6%	[110]
PPZ	-	-	30.1	0.84	1800 h, 0.5 mA cm^{-2}/ 0.5 mAh cm^{-2}	Zn||PANI@TOC, 100, 2 mA cm^{-2}, —	[112]
PMZA	-	-	71.17	0.912	1800 h, 0.5 mA cm^{-2}/ 0.5 mAh cm^{-2}	Zn||NVO, 7000, 5 A g^{-1}, 100%	[114]
ATAC/EG/ PAA/$Zn(OTF)_2$	0.08	570	7.5	-	-	Zn||CC/Pt/C/RuO2, 127 h, 0.1 mA cm^{-2}, —	[115]
PAA/CNF	0.04	~220	32	-	4600 h, 0.5 mA cm^{-2}/ 0.25 mAh cm^{-2}, at −20 °C	Zn||FeHCF, 3000 h, 4 A g^{-1}, 84.1%	[116]
PAA/Al_2O_3	0.1	~800	186	-	-	Zn||Co_3O_4/C/Ni, 384 h, 2 mA cm^{-2}, —	[117]
DPR/PAA	0.38	1450	23.24	-	>1700 h, 5 mA cm^{-2}/ 5 mAh cm^{-2}	Zn||MnO_2, 1000 h, 3 A g^{-1}, 81.3%	[118]

4. Outlook

HPEs, characterized by their hybrid solid–liquid synergistic behavior, tunable functional groups, and excellent interfacial adaptability, represent a highly promising approach to addressing key challenges in aqueous ZIBs. By confining water molecules and enabling directional ion transport through tailored polymer networks, HPEs not only suppress side

reactions such as dendrite formation and hydrogen evolution but also enhance interfacial stability and mechanical resilience. Although certain progress has been made, the technological maturity of HPEs remains insufficient for large-scale commercial applications. Bridging this gap requires concerted efforts to optimize material design, interface engineering, and fabrication strategies, as outlined in the following key directions for future research.

4.1. Rational Design of High-Performance Multifunctional HPEs

HPEs, which combine the structural stability of solid-state electrolytes with the favorable interfacial contact of liquid electrolytes, show significant potential for enhancing the cycle life of aqueous ZIBs. Nevertheless, their long-term electrochemical stability is still hindered by several intrinsic challenges. (i) Water retention and structural stability. Water evaporation—especially at elevated temperatures—causes HPE dehydration, leading to a sharp drop in ionic conductivity, loss of elasticity, and increased interfacial resistance. To alleviate this issue, humectants such as glycerol and ionic liquids, or water-retentive double-network architectures rich in hydrophilic or hydrogen-bonding groups, have been introduced to maintain hydration and structural integrity [101,110]. (ii) Dendrite suppression and mechanical reinforcement. Although HPEs exhibit good mechanical strength, insufficient modulus or uneven ion flux can still allow Zn dendrites to penetrate the electrolyte, resulting in short circuits. Strategies to address this include enhancing the modulus via nanocomposite or structural design [110,117], introducing zincophilic interfacial layers on the Zn anode [123], and incorporating functional groups (e.g., -SO_3^-) to regulate Zn^{2+} flux and deposition morphology [124]. Furthermore, in situ polymerization to construct an integrated Zn/HPE interface effectively eliminates interfacial gaps and promotes uniform Zn plating/stripping [125]. (iii) Suppression of parasitic reactions and polymer degradation. The presence of free water molecules can trigger parasitic hydrogen evolution and corrosion, consuming active materials and increasing impedance. Introducing strongly polar additives (e.g., glycerol, formamide, proline) can weaken the hydrogen-bond network among water molecules, converting free water into electrochemically inactive bound water [126,127]. Additionally, oxidation-resistant polymer backbones are required to mitigate electrochemical and radical-induced degradation under high-voltage operation [128]. (iv) Interfacial adaptability and mechanical compliance. Substantial electrode volume changes during cycling—such as Zn dissolution/deposition and cathode phase transitions (e.g., in vanadium- or manganese-based oxides)—can lead to interfacial mismatch. Developing HPEs with strong adhesiveness and self-healing capability is thus critical to maintaining interfacial integrity and long-term performance [107,115]. Future research should focus on synergistically combining these strategies to develop multifunctional HPE systems that simultaneously offer high water retention, mechanical robustness, adaptive interfacial contact, and electrochemical stability.

Future research should focus on synergistic material design to realize multifunctional HPEs with high water retention, mechanical robustness, interfacial adaptability, and electrochemical stability. Next-generation HPEs are expected to emerge from the rational design of novel polymer monomers, advanced crosslinking strategies, and composite architectures incorporating nanomaterials such as MOFs, COFs, MXenes, and biomacromolecules. Ideal HPEs should deliver ultrahigh ionic conductivity (even under low temperatures or high current densities), high mechanical strength (up to the MPa level), wide electrochemical stability windows, low Zn^{2+} deposition overpotentials, and self-healing, adhesive interfaces. In addition, elucidating structure–property relationships—including the effects of functional group type/density (e.g., sulfonic or phosphoric acid groups, heteroatoms) and network topology (e.g., gradient, biomimetic, or heterogeneous architectures)—will

be essential for guiding rational HPE design. Finally, the development of intelligent, stimuli-responsive HPEs (e.g., pH-, stress-, or temperature-responsive systems) could enable adaptive self-regulation and protection under complex operation conditions such as mechanical deformation, thermal fluctuations, or local overpotential.

4.2. In-Depth Understanding of Ion Transport and Interfacial Mechanisms

Comprehensive elucidation of ion transport, interfacial dynamics, and dendrite suppression mechanisms is essential for the rational design of HPEs. In situ and operando characterization techniques play a pivotal role in uncovering these fundamental processes. For instance, synchrotron radiation X-ray diffraction enables real-time tracking of phase evolution in cathode materials (e.g., V_2O_5 or MnO_2) during Zn^{2+} insertion/extraction, thereby revealing structural reversibility and phase transition mechanisms [129]; X-ray absorption spectroscopy further probes valence state changes and local coordination environments, elucidating the electronic structure evolution and oxidation-state regulation during cycling [129]. In situ Fourier transform infrared spectroscopy and Raman spectroscopy provide molecular-level insights into interfacial chemical species (such as water molecules and sulfate ions) and solvation structures, clarifying Zn^{2+} coordination, solvation–desolvation behavior, and interfacial reaction kinetics [130,131]. Moreover, in situ optical microscopy directly visualizes zinc deposition and dendrite growth processes, supplying real-time evidence for deposition uniformity and dendrite inhibition [132]. Electrochemical quartz crystal microbalance quantitatively measures mass changes at the interface, enabling evaluation of Zn deposition/dissolution reversibility and Coulombic efficiency [133]. High-resolution in situ scanning/transmission electron microscopy reveals microstructural evolution and zinc morphology at the nanoscale, supporting mechanistic understanding of dendrite initiation and growth [132]. Collectively, these advanced techniques provide multi-scale insights into zinc deposition behavior, SEI formation, solvation structure modulation, and parasitic reaction suppression—laying a strong foundation for performance optimization and durability enhancement of aqueous Zn-ion batteries. Beyond experimental characterization, coupling these methods with molecular dynamics (MD) simulations and first-principles calculations is critical for exploring the dynamic behavior of confined water molecules and solvated ions within polymer networks. Such approaches can elucidate ion transport pathways, diffusion coefficients, and desolvation activation barriers for Zn^{2+} and counterions (e.g., SO_4^{2-}, Cl^-). Moreover, atomistic-level understanding of interfacial processes—such as Zn^{2+} nucleation, deposition/dissolution, interfacial charge transfer, and H^+ participation—will clarify the origins of parasitic reactions (e.g., hydrogen evolution, corrosion, gas formation) and guide the design of more stable interfaces. Ultimately, integrating in situ characterization with multi-scale theoretical modeling will enable quantitative correlation between structure, transport, and electrochemical performance. Such predictive frameworks are indispensable for accelerating the rational optimization of next-generation HPEs with superior ion transport, interfacial stability, and dendrite-free operation.

4.3. Interface Engineering and Stability Enhancement

To mitigate interfacial degradation caused by byproducts accumulation during long-term cycling, increased contact resistance, and HPE swelling/drying, novel interfacial modification layers should be developed. These layers can be formed in situ via electrochemical polymerization, self-assembly, or photo/thermal-initiated curing. Integrated electrode–electrolyte structures fabricated through pre-gelation, 3D printing or other monolithic methods may offer improved mechanical and electrochemical compatibility. Concurrently, degradation mechanisms under extreme conditions (e.g., high temperature, humidity, or

deep cycling) should be systematically, and countermeasures developed to extend the operational lifespan and environmental adaptability of HPE-based ZIBs.

4.4. Scalable Fabrication and Sustainability

Transitioning HPEs for ZIBs from laboratory-scale research to practical deployment requires scalable, cost-effective, and environmentally friendly manufacturing techniques. Although continuous fabrication techniques such as roll-to-roll coating and 3D printing show promise, significant bottlenecks persist. Achieving uniform thickness in large-area HPE films remains challenging, as minor variations can induce heterogeneous ion flux and accelerate localized dendrite growth. While roll-to-roll coating theoretically supports line speeds up to 5 m min^{-1}, maintaining high-precision thickness control often necessitates nano-patterned molds or in situ monitoring systems, increasing equipment costs by more than 30% [92]. Furthermore, the typical crosslinking time (>30 min per batch) must be shortened to <5 min to achieve industrially viable throughput, while material utilization efficiency for low-viscosity precursors—often below 60%—must also be improved to reduce production waste [134]. From a sustainability perspective, establishing closed-loop recycling systems is essential to enhance the life-cycle performance of ZIBs employing HPEs. However, several technical and economic obstacles remain. De-crosslinking strategies such as enzymatic catalysis can achieve high depolymerization efficiencies (>90%) but suffer from long processing times (48–72 h) and high enzyme costs, which can account for up to 30% of the recycled material's value. Efficient component recovery is another major challenge—purifying high-purity Zn salts (>70%) from spent HPEs typically requires energy-intensive separation steps [135]. Additionally, regenerated HPEs generally exhibit a 15–30% reduction in ionic conductivity and a 20% decrease in mechanical strength after the first recycling cycle [134]. Although life-cycle assessments suggest that recycling can reduce overall carbon emissions by up to 50% compared with virgin material use, the recycling process itself contributes approximately 35% of the total carbon footprint of the regenerated electrolyte. Therefore, future efforts should prioritize process intensification and energy-efficient recycling protocols to simultaneously reduce manufacturing costs, improve material utilization, and minimize environmental impact. Integrating scalable fabrication, rapid crosslinking chemistry, high-yield material recovery, and circular recycling frameworks will be critical to realizing sustainable, large-scale implementation of HPE-based aqueous ZIBs.

4.5. Advanced Battery Configurations and Expanded Application

Integration high-performance HPEs with high-capacity cathode materials (e.g., high-voltage Mn-based compounds, organic electrodes) and optimized anode architectures (e.g., 3D structured Zn) will enable ZIBs with high energy and power densities and long cycle life. The intrinsic flexibility of HPEs supports the development of next-generation batteries that are flexible, stretchable, wearable, and even self-healing, expanding their potential applications to wearable electronics, implantable medical devices, and smart textiles.

5. Conclusions

HPEs represent a promising approach to overcoming the intrinsic challenges of aqueous ZIBs. By combining solid–liquid hybrid characteristics, tunable functional groups, and robust interfacial adaptability, HPEs effectively suppress Zn dendrite formation, minimize hydrogen evolution and corrosion, and enhance ionic conductivity and mechanical resilience. PAM-, PVA-, and PAA-based HPEs each demonstrate unique advantages, such as stretchability, anti-freezing capability, self-healing, and dynamic Zn^{2+} coordination. Low-temperature strategies further expand HPE applicability, ensuring stable cycling and

high conductivity down to –70 °C. Despite these advances, challenges remain in long-term electrochemical stability, scalable fabrication, and sustainable recycling. Overall, HPEs provide a versatile platform for safe, durable, and high-performance aqueous ZIBs, laying the foundation for future flexible and wearable energy storage technologies.

Author Contributions: Conceptualization, Z.Z. and Y.S.; methodology, Z.Z., S.X. and J.L.; formal analysis, X.T., L.L. and Q.S.; investigation, Z.Z. and L.W.; resources, Z.Z., S.X. and J.L.; data curation, Z.Z. and L.W.; writing—original draft preparation, Z.Z.; writing—review and editing, Y.S.; visualization, supervision, Y.S. and J.S.; project administration, Y.S. and J.S. All authors have read and agreed to the published version of the manuscript.

Funding: This research funded by the National Natural Science Foundation of China (Nos. 52062004, 52372185), Guizhou Province's High-level Innovative Talents (QKHPTRC-GCC [2022]013-1), Guizhou Province's Advanced Electrochemical Energy Storage Devices and Key Materials Innovation Team (QJJ [2023]054), and Guizhou Province's Advanced Electrochemical Energy Storage Devices and Key Materials Scientific and Technological Innovation Talent Team (QKHPTRC-CXTD [2023]016).

Data Availability Statement: No new data were created or analyzed in this study.

Conflicts of Interest: The authors declare no conflicts of interest.

References

1. Jha, A.; Misra, A.K. Consequences of shifting to renewable energy on atmospheric carbon dioxide: A mathematical model. *J. Appl. Math. Comput.* **2024**, *70*, 4851–4876. [CrossRef]
2. Kosowski, P. From Fossil Fuels to Renewables: Clustering European Primary Energy Production from 1990 to 2022. *Energies* **2024**, *17*, 5596. [CrossRef]
3. Sun, H.; Xiang, X.; Wang, X.; Tsai, H.S.; Feng, W. Advanced photo-rechargeable lithium- and zinc-ion batteries: Progress and prospect. *J. Power Sources* **2024**, *598*, 234204. [CrossRef]
4. Arsad, A.Z.; Hannan, M.A.; Al-Shetwi, A.Q.; Begum, R.A.; Hossain, M.J.; Ker, P.J.; Mahlia, T.M.I. Hydrogen electrolyser technologies and their modelling for sustainable energy production: A comprehensive review and suggestions. *Int. J. Hydrogen Energy* **2023**, *48*, 27841–27871. [CrossRef]
5. Ruan, S.; Luo, D.; Li, M.; Wang, J.; Ling, L.; Yu, A.; Chen, Z. Synthesis and functionalization of 2D nanomaterials for application in lithium-based energy storage systems. *Energy Storage Mater.* **2021**, *38*, 200–230. [CrossRef]
6. Mo, J.Y.; Jeon, W. The Impact of Electric Vehicle Demand and Battery Recycling on Price Dynamics of Lithium-Ion Battery Cathode Materials: A Vector Error Correction Model (VECM) Analysis. *Sustainability* **2018**, *10*, 2870. [CrossRef]
7. Li, S.; Zhou, S.; Zhao, S.; Jin, T.; Zhong, M.; Cen, Z.; Gao, P.; Yan, W.; Ling, M. Room Temperature Resistive Hydrogen Sensor for Early Safety Warning of Li-Ion Batteries. *Chemosensors* **2023**, *11*, 344. [CrossRef]
8. Forsyth, M.; Porcarelli, L.; Wang, X.; Goujon, N.; Mecerreyes, D. Innovative Electrolytes Based on Ionic Liquids and Polymers for Next-Generation Solid -State Batteries. *Acc. Chem. Res.* **2019**, *52*, 686–694. [CrossRef]
9. Meng, R.; Li, H.; Lu, Z.; Zhang, C.; Wang, Z.; Liu, Y.; Wang, W.; Ling, G.; Kang, F.; Yang, Q.-H. Tuning Zn-Ion Solvation Chemistry with Chelating Ligands toward Stable Aqueous Zn Anodes. *Adv. Mater.* **2022**, *34*, 2200677. [CrossRef]
10. Yang, J.L.; Li, J.; Zhao, J.W.; Liu, K.; Yang, P.; Fan, H.J. Stable Zinc Anodes Enabled by a Zincophilic Polyanionic Hydrogel Layer. *Adv. Mater.* **2022**, *34*, 2202382. [CrossRef]
11. Zhou, L.; Wang, F.; Yang, F.; Liu, X.; Yu, Y.; Zheng, D.; Lu, X. Unshared Pair Electrons of Zincophilic Lewis Base Enable Long-life Zn Anodes under "Three High" Conditions. *Angew. Chem.-Int. Ed.* **2022**, *61*, e202208051. [CrossRef] [PubMed]
12. Perez-Antolin, D.; Saez-Bernal, I.; Colina, A.; Ventosa, E. Float-charging protocol in rechargeable Zn-MnO_2 batteries: Unraveling the key role of Mn^{2+} additives in preventing spontaneous pH changes. *Electrochem. Commun.* **2022**, *138*, 107271. [CrossRef]
13. Tang, B.; Shan, L.; Liang, S.; Zhou, J. Issues and opportunities facing aqueous zinc-ion batteries. *Energy Environ. Sci.* **2019**, *12*, 3288–3304. [CrossRef]
14. Yang, S.; Du, H.; Li, Y.; Wu, X.; Xiao, B.; He, Z.; Zhang, Q.; Wu, X. Advances in the structure design of substrate materials for zinc anode of aqueous zinc ion batteries. *Green Energy Environ.* **2023**, *8*, 1531–1552. [CrossRef]
15. Naveed, A.; Yang, H.; Shao, Y.; Yang, J.; Yanna, N.; Liu, J.; Shi, S.; Zhang, L.; Ye, A.; He, B.; et al. A Highly Reversible Zn Anode with Intrinsically Safe Organic Electrolyte for Long-Cycle-Life Batteries. *Adv. Mater.* **2019**, *31*, 1900668. [CrossRef]
16. Naveed, A.; Yang, H.; Yang, J.; Nuli, Y.; Wang, J. Highly Reversible and Rechargeable Safe Zn Batteries Based on a Triethyl Phosphate Electrolyte. *Angew. Chem. Int. Ed.* **2019**, *58*, 2760–2764. [CrossRef]

17. Zhu, K.; Niu, X.; Xie, W.; Yang, H.; Jiang, W.; Ma, M.; Yang, W. An integrated Janus hydrogel with different hydrophilicities and gradient pore structures for high-performance zinc-ion batteries. *Energy Environ. Sci.* **2024**, *17*, 4126–4136. [CrossRef]
18. Wu, K.; Cui, J.; Yi, J.; Liu, X.; Ning, F.; Liu, Y.; Zhang, J. Biodegradable Gel Electrolyte Suppressing Water-Induced Issues for Long-Life Zinc Metal Anodes. *ACS Appl. Mater. Interfaces* **2022**, *14*, 34612–34619. [CrossRef]
19. Li, X.; Wang, D.; Ran, F. Key approaches and challenges in fabricating advanced flexible zinc-ion batteries with functional hydrogel electrolytes. *Energy Storage Mater.* **2023**, *56*, 351–393. [CrossRef]
20. Zhang, L.; Zhang, T.; Xin, W.; Peng, H.; Yan, Z.; Zhu, Z. Additive engineering for a hydrophilic/zincophilic polymeric layer towards dendrite-free zinc anode. *Mater. Today Energy* **2022**, *29*, 101130. [CrossRef]
21. Qi, R.; Tang, W.; Shi, Y.; Teng, K.; Deng, Y.; Zhang, L.; Zhang, J.; Liu, R. Gel Polymer Electrolyte toward Large-Scale Application of Aqueous Zinc Batteries. *Adv. Funct. Mater.* **2023**, *33*, 2306052. [CrossRef]
22. Sun, M.; Wang, Z.; Jiang, J.; Wang, X.; Yu, C. Gelation mechanisms of gel polymer electrolytes for zinc-based batteries. *Chin. Chem. Lett.* **2024**, *35*, 109393. [CrossRef]
23. Vandeginste, V.; Wang, J. A Review of the Synthesis of Biopolymer Hydrogel Electrolytes for Improved Electrode-Electrolyte Interfaces in Zinc-Ion Batteries. *Energies* **2024**, *17*, 310. [CrossRef]
24. Gong, Y.Y.; Zhang, P.T.; Fan, S.; Cai, M.H.; Hu, J.T.; Luo, Z.Y.; Mi, H.W.; Jiang, X.T.; Zhang, Q.L.; Ren, X.Z. Polypyrrole pre-intercalation engineering-induced NH^{4+} removal in tunnel ammonium vanadate toward high-performance zinc ion batteries. *J. Colloid Interface Sci.* **2024**, *664*, 168–177. [CrossRef]
25. Ji, J.; Cheng, F.; Cai, W.; Ji, Y.; Liu, J.; Wang, Y.; Cai, C.; Fu, Y. Constructing ion "Tongs" and double-network for cellulose-based semi-solid electrolytes towards dendrite-free dual-ion batteries. *Chem. Eng. J.* **2024**, *482*, 149172. [CrossRef]
26. Lee, C.J.; Wu, H.; Hu, Y.; Young, M.; Wang, H.; Lynch, D.; Xu, F.; Cong, H.; Cheng, G. Ionic Conductivity of Polyelectrolyte Hydrogels. *ACS Appl. Mater. Interfaces* **2018**, *10*, 5845–5852. [CrossRef]
27. Chen, J.; Zhai, Y.J.; Li, Y.J.; Zhang, X.Y.; Zhang, X.Q.; Chen, Y.X.; Zeng, Y.X.; Wu, X.Q.; Zheng, Q.J.; Lam, K.H.; et al. Optimizing Interplanar Spacing, Oxygen Vacancies and Micromorphology via Lithium-Ion Pre-Insertion into Ammonium Vanadate Nanosheets for Advanced Cathodes in Aqueous Zinc-Ion Batteries. *Small* **2024**, *20*, 2309412. [CrossRef] [PubMed]
28. Jeon, O.S.; Ko, E.S.; Park, Y.Y.; Hong, D.; Lee, S.H.; Jeon, Y.P.; La, Y.; Kim, S.; Lee, I.-S.; Park, G.S.; et al. Hygroscopic and Malleable Dough-Type Zn-Air Battery in a Dry Condition Utilizing Deliquescence. *Adv. Energy Mater.* **2023**, *13*, 2300285. [CrossRef]
29. Yang, M.; Zhu, J.; Bi, S.; Wang, R.; Niu, Z. A Binary Hydrate-Melt Electrolyte with Acetate-Oriented Cross-Linking Solvation Shells for Stable Zinc Anodes. *Adv. Mater.* **2022**, *34*, 2201744. [CrossRef]
30. Fu, C.; Wang, Y.; Lu, C.; Zhou, S.; He, Q.; Hu, Y.; Feng, M.; Wan, Y.; Lin, J.; Zhang, Y.; et al. Modulation of hydrogel electrolyte enabling stable zinc metal anode. *Energy Storage Mater.* **2022**, *51*, 588–598. [CrossRef]
31. Wu, Y.; Li, Y.; Wang, Y.; Liu, Q.; Chen, Q.; Chen, M. Advances and prospects of PVDF based polymer electrolytes. *J. Energy Chem.* **2022**, *64*, 62–84. [CrossRef]
32. Mishra, K.; Yadav, N.; Hashmi, S.A. Recent progress in electrode and electrolyte materials for flexible sodium-ion batteries. *J. Mater. Chem. A* **2020**, *8*, 22507–22543. [CrossRef]
33. Bai, L.; Ghiassinejad, S.; Brassinne, J.; Fu, Y.; Wang, J.; Yang, H.; Vlad, A.; Minoia, A.; Lazzaroni, R.; Gohy, J.-F. High Salt-Content Plasticized Flame-Retardant Polymer Electrolytes. *ACS Appl. Mater. Interfaces* **2021**, *13*, 44844–44859. [CrossRef]
34. Chen, Q.; Zhao, J.; Chen, Z.; Jin, Y.; Chen, J. High voltage and self-healing zwitterionic double-network hydrogels as electrolyte for zinc-ion hybrid supercapacitor/battery. *Int. J. Hydrogen Energy* **2022**, *47*, 23909–23918. [CrossRef]
35. Chen, Q.; Wang, L.; Chen, J. Low-Temperature and High-Voltage-Tolerant Zinc-Ion Hybrid Supercapacitor Based on a Hydrogel Electrolyte. *Chemelectrochem* **2022**, *9*, e202200070. [CrossRef]
36. Zhang, H.; Liu, X.; Qin, B.; Passerini, S. Electrochemical intercalation of anions in graphite for high-voltage aqueous zinc battery. *J. Power Sources* **2020**, *449*, 227594. [CrossRef]
37. Yang, Y.; Guo, S.; Pan, Y.; Lu, B.; Liang, S.; Zhou, J. Dual mechanism of ion (de)intercalation and iodine redox towards advanced zinc batteries. *Energy Environ. Sci.* **2023**, *16*, 2358–2367. [CrossRef]
38. Fan, H.; Wang, K.; Xu, Z. Tungsten Doping of Two-Dimensional VO_2. Nanoribbons for Rapid Zinc Ion Storage Channels. *Chemistryselect* **2024**, *9*, e202401229. [CrossRef]
39. Zhao, Q.; Huang, X.; Zhou, M.; Ju, Z.; Sun, X.; Sun, Y.; Huang, Z.; Li, H.; Ma, T. Proton Insertion Promoted a Polyfurfural/MnO_2 Nanocomposite Cathode for a Rechargeable Aqueous Zn-MnO_2 Battery. *ACS Appl. Mater. Interfaces* **2020**, *12*, 36072–36081. [CrossRef]
40. Hou, Z.; Zhang, X.; Dong, M.; Xiong, Y.; Zhang, Z.; Ao, H.; Liu, M.; Zhu, Y.; Qian, Y. A large format aqueous rechargeable LiMn2O4/Zn battery with high energy density and long cycle life. *Sci. China Mater.* **2021**, *64*, 783–788. [CrossRef]
41. Cui, S.; Zhang, D.; Gan, Y. Traditional Electrochemical Zn^{2+} Intercalation/Extraction Mechanism Revisited: Unveiling Ion-Exchange Mediated Irreversible Zn^{2+} Intercalation for the δ-MnO_2 Cathode in Aqueous Zn Ion Batteries. *Adv. Energy Mater.* **2024**, *14*, 2302655. [CrossRef]

42. Li, D.; Ye, Z.; Ding, H.; Li, J.; Huang, H.; Yang, Z.; Su, J.; Zhu, J.; Zhang, W. Boosting proton intercalation via sulfur anion doping in V_2O_3 cathode materials towards high capacity and rate performance of aqueous zinc ion batteries. *Energy Storage Mater.* **2024**, *71*, 103635. [CrossRef]
43. Li, F.; Ma, H.; Sheng, H.; Wang, Z.; Qi, Y.; Wan, D.; Shao, M.; Yuan, J.; Li, W.; Wang, K.; et al. Interlayer and Phase Engineering Modifications of K-MoS_2@C Nanoflowers for High-Performance Degradable Zn-Ion Batteries. *Small* **2024**, *20*, 2306276. [CrossRef] [PubMed]
44. Sada, K.; Darga, J.; Manthiram, A. Challenges and Prospects of Sodium-Ion and Potassium-Ion Batteries for Mass Production. *Adv. Energy Mater.* **2023**, *13*, 2302321. [CrossRef]
45. Liu, B.; Zhao, R.; Zhang, Q.; Ali, U.; Li, Y.; Hao, Y.; Jia, H.; Li, Y.; Zeng, G.; Sun, M.; et al. Ultrafine manganese hexacyanoferrate with low defects regulated by potassium polyacrylate for high-performance aqueous Zn-ion batteries. *J. Energy Storage* **2023**, *72*, 108535. [CrossRef]
46. Sun, W.; Wang, F.; Hou, S.; Yang, C.; Fan, X.; Ma, Z.; Gao, T.; Han, F.; Hu, R.; Zhu, M.; et al. Zn/MnO_2 Battery Chemistry With H^+ and Zn^{2+} Coinsertion. *J. Am. Chem. Soc.* **2017**, *139*, 9775–9778. [CrossRef]
47. Zhang, Y.X.; Deng, X.Y.; Ma, Z.Z.; Wang, X.G. Competition-cooperation mechanism between adsorption and conversion reaction for a novel SnS_2@C composite cathode in zinc-ion batteries. *J. Alloys Compd.* **2025**, *1014*, 178855. [CrossRef]
48. Wang, Y.; Wu, N.; Qi, Y.; Zhu, Z.; Zhang, T.; Han, X.; Li, S.; Wu, J.; Qiu, J. Hollow iron carbides via nanoscale Kirkendall cavitation process for zinc-air batteries. *Appl. Surf. Sci.* **2022**, *585*, 152569. [CrossRef]
49. Li, L.; Cheng, S.; Deng, L.; Liu, T.; Dong, W.; Liu, Y.; Huang, L.; Yao, H.; Ji, X. Effective Solution toward the Issues of Zn-Based Anodes for Advanced Alkaline Ni-Zn Batteries. *ACS Appl. Mater. Interfaces* **2023**, *15*, 3953–3960. [CrossRef]
50. Li, Z.; Chen, X.; Zhang, R.; Shen, T.; Sun, J.; Hu, Z.; Li, L.; Yang, L.; Yu, H.Y. Advanced cellulose-based materials toward stabilizing zinc anodes. *Sci. China Chem.* **2024**, *67*, 1465–1484. [CrossRef]
51. Li, M.; Lai, C.; He, X.; Zhang, Z.; Hu, J.; Shan, B.; Jiang, K.; Wang, K. Texturing Crystal Plane of Zinc Metal via Cleavage Fracture for a Dendrite-Free Zinc Anode. *ACS Appl. Mater. Interfaces* **2022**, *14*, 49719–49729. [CrossRef]
52. Zhang, Q.; Liu, X.; Zhu, X.; Wan, Y.; Zhong, C. Interface Engineering of Zinc Electrode for Rechargeable Alkaline Zinc-Based Batteries. *Small Methods* **2023**, *7*, 2201277. [CrossRef] [PubMed]
53. Liu, Y.; Chen, Y.; Zhang, X.; Lin, C.; Zhang, H.; Miao, X.; Lin, J.; Chen, S.; Zhang, Y. A high-voltage aqueous rechargeable zinc-polyaniline hybrid battery achieved by decoupling alkali-acid electrolyte. *Chem. Eng. J.* **2022**, *444*, 136478. [CrossRef]
54. Qu, W.; Cai, Y.; Chen, B.; Zhang, M. Heterointerface Engineering-Induced Oxygen Defects for the Manganese Dissolution Inhibition in Aqueous Zinc Ion Batteries. *Energy Environ. Mater.* **2024**, *7*, 12645. [CrossRef]
55. Wang, C.; Xiao, B.H.; Huang, J.; Xiao, K.; Liu, Z.Q. Microstructure Strain of $ZnMn_2O_4$ Spinel by Regulation of Tetrahedral Sites for High-Performance Aqueous Zinc-Ion Battery. *Adv. Funct. Mater.* **2024**, *34*, 2405680. [CrossRef]
56. Juran, T.R.; Young, J.; Smeu, M. Density Functional Theory Modeling of MnO_2 Polymorphs as Cathodes for Multivalent Ion Batteries. *J. Phys. Chem. C* **2018**, *122*, 8788–8795. [CrossRef]
57. Wu, X.; Xiang, Y.; Peng, Q.; Wu, X.; Li, Y.; Tang, F.; Song, R.; Liu, Z.; He, Z.; Wu, X. Green-low-cost rechargeable aqueous zinc-ion batteries using hollow porous spinel $ZnMn_2O_4$ as the cathode material. *J. Mater. Chem. A* **2017**, *5*, 17990–17997. [CrossRef]
58. Wu, X.; Li, Y.; Li, C.; He, Z.; Xiang, Y.; Xiong, L.; Chen, D.; Yu, Y.; Sun, K.; He, Z.; et al. The electrochemical performance improvement of $LiMn_2O_4$/Zn based on zinc foil as the current collector and thiourea as an electrolyte additive. *J. Power Sources* **2015**, *300*, 453–459. [CrossRef]
59. Hoang, T.K.A.; Doan, T.N.L.; Cho, J.H.; Su, J.Y.J.; Lee, C.; Lu, C.; Chen, P. Sustainable Gel Electrolyte Containing Pyrazole as Corrosion Inhibitor and Dendrite Suppressor for Aqueous Zn/$LiMn_2O_4$ Battery. *ChemSusChem* **2017**, *10*, 2816–2822. [CrossRef]
60. Cui, J.; Wu, X.; Yang, S.; Li, C.; Tang, F.; Chen, J.; Chen, Y.; Xiang, Y.; Wu, X.; He, Z. Cryptomelane-Type KMn_8O_{16} as Potential Cathode Material—For Aqueous Zinc Ion Battery. *Front. Chem.* **2018**, *6*, 600352. [CrossRef]
61. Zhao, Y.; Zhu, Y.; Zhang, X. Challenges and perspectives for manganese-based oxides for advanced aqueous zinc-ion batteries. *InfoMat* **2020**, *2*, 237–260. [CrossRef]
62. Wei, T.; Li, Q.; Yang, G.; Wang, C. An electrochemically induced bilayered structure facilitates long-life zinc storage of vanadium dioxide. *J. Mater. Chem. A* **2018**, *6*, 8006–8012. [CrossRef]
63. Tang, B.; Zhou, J.; Fang, G.; Guo, S.; Guo, X.; Shan, L.; Tang, Y.; Liang, S. Structural Modification of V_2O_5 as High-Performance Aqueous Zinc-Ion Battery Cathode. *J. Electrochem. Soc.* **2019**, *166*, A480–A486. [CrossRef]
64. Xu, X.; Xiong, F.; Meng, J.; Wang, X.; Niu, C.; An, Q.; Mai, L. Vanadium-Based Nanomaterials: A Promising Family for Emerging Metal-Ion Batteries. *Adv. Funct. Mater.* **2020**, *30*, 1904398. [CrossRef]
65. Dai, X.; Wan, F.; Zhang, L.; Cao, H.; Niu, Z. Freestanding graphene/VO_2 composite films for highly stable aqueous Zn-ion batteries with superior rate performance. *Energy Storage Mater.* **2019**, *17*, 143–150. [CrossRef]
66. Zhang, L.; Chen, L.; Zhou, X.; Liu, Z. Towards High-Voltage Aqueous Metal-Ion Batteries Beyond 1.5 V: The Zinc/Zinc Hexacyanoferrate System. *Adv. Energy Mater.* **2015**, *5*, 1501125. [CrossRef]

67. Trocoli, R.; La Mantia, F. An Aqueous Zinc-Ion Battery Based on Copper Hexacyanoferrate. *Chemsuschem* **2015**, *8*, 481–485. [CrossRef]
68. Li, Q.; Ma, K.; Hong, C.; Yang, Z.; Qi, C.; Yang, G.; Wang, C. High-voltage K/Zn dual-ion battery with 100,000-cycles life using zero-strain ZnHCF cathode. *Energy Storage Mater.* **2021**, *42*, 715–722. [CrossRef]
69. Zeng, X.; Hao, J.; Wang, Z.; Mao, J.; Guo, Z. Recent progress and perspectives on aqueous Zn-based rechargeable batteries with mild aqueous electrolytes. *Energy Storage Mater.* **2019**, *20*, 410–437. [CrossRef]
70. Kim, S.; Oguchi, H.; Toyama, N.; Sato, T.; Takagi, S.; Otomo, T.; Arunkumar, D.; Kuwata, N.; Kawamura, J.; Orimo, S.-i. A complex hydride lithium superionic conductor for high-energy-density all-solid-state lithium metal batteries. *Nat. Commun.* **2019**, *10*, 1081–1092. [CrossRef]
71. Lu, Y.; Hou, X.; Miao, L.; Li, L.; Shi, R.; Liu, L.; Chen, J. Cyclohexanehexone with Ultrahigh Capacity as Cathode Materials for Lithium-Ion Batteries. *Angew. Chem. Int. Ed.* **2019**, *58*, 7020–7024. [CrossRef]
72. Sheng, X.; Zhang, Z.; Ding, T.; Liao, J.; Zhou, X. Recent Advances in Amorphous $FePO_4$ for Sodium-Ion Battery Cathodes. *Chem. J. Chin. Univ. Chin.* **2023**, *44*, e200336.
73. Wu, Y.; Shi, M.; Luo, D.; Zhang, Z.; Li, Z.; Cheng, Z.; Kang, X. Synergetic effect of TiO_2 coating and oxygen vacancy boosting $LiMn_2O_4$ cathode for stable aqueous zinc-ion batteries. *J. Electroanal. Chem.* **2023**, *943*, 117597. [CrossRef]
74. Yesibolati, N.; Umirov, N.; Koishybay, A.; Omarova, M.; Kurmanbayeva, I.; Zhang, Y.; Zhao, Y.; Bakenov, Z. High Performance $Zn/LiFePO_4$ Aqueous Rechargeable Battery for Large Scale Applications. *Electrochim. Acta* **2015**, *152*, 505–511. [CrossRef]
75. Mainar, A.R.; Leonet, O.; Bengoechea, M.; Boyano, I.; de Meatza, I.; Kvasha, A.; Guerfi, A.; Alberto Blazquez, J. Alkaline aqueous electrolytes for secondary zinc-air batteries: An overview. *Int. J. Energy Res.* **2016**, *40*, 1032–1049. [CrossRef]
76. Santos, F.; Tafur, J.P.; Abad, J.; Fernandez Romero, A.J. Structural modifications and ionic transport of PVA-KOH hydrogels applied in Zn/Air batteries. *J. Electroanal. Chem.* **2019**, *850*, 113380. [CrossRef]
77. Zhou, M.; Fu, C.Y.; Qin, L.P.; Ran, Q.; Guo, S.; Fang, G.Z.; Lang, X.Y.; Jiang, Q.; Liang, S.Q. Intrinsic structural optimization of zinc anode with uniform second phase for stable zinc metal batteries. *Energy Storage Mater.* **2022**, *52*, 161–168. [CrossRef]
78. Chen, A.; Zhang, Y.; Li, Q.; Liang, G.; Yang, S.; Huang, Z.; Yang, Q.; Hu, H.; Li, X.; Chen, Z.; et al. An immiscible phase-separation electrolyte and interface ion transfer electrochemistry enable zinc/lithium hybrid batteries with a 3.5 V-class operating voltage. *Energy Environ. Sci.* **2023**, *16*, 4054–4064. [CrossRef]
79. Deng, R.; He, Z.; Chu, F.; Lei, J.; Cheng, Y.; Zhou, Y.; Wu, F. An aqueous electrolyte densified by perovskite $SrTiO_3$ enabling high-voltage zinc-ion batteries. *Nat. Commun.* **2023**, *14*, 4981–4987. [CrossRef]
80. Alawi, M.J.; Gamal, H.; Rashad, M.; Alziyadi, M.O.; Shalaby, M.S. Zinc-ion batteries: Drawbacks, opportunities, and optimization performance for sustainable energy storage. *J. Alloys Compd.* **2025**, *1012*, 178455. [CrossRef]
81. Cui, J.; Chen, Y.; Dong, Y.; Zhang, H.; Ivey, D.G. Sodium succinate as functional electrolyte additive to achieve highly reversible zinc-ion batteries. *J. Mater. Chem. A* **2024**, *12*, 28475–28485. [CrossRef]
82. Liu, L.; Liu, Y.; Zhang, L.; Wang, R.; Ma, Q.; Xiong, P.; Zhang, C. Minireview and Perspectives on Functional Electrolyte Additives for Aqueous Zinc-Ion Batteries. *Energy Fuels* **2024**, *38*, 15998–16009. [CrossRef]
83. Wu, L.; Li, Z.; Xiang, Y.; Dong, W.; Qi, X.; Ling, Z.; Xu, Y.; Wu, H.; Levi, M.D.; Shpigel, N.; et al. Revisiting the Charging Mechanism of α-MnO_2 in Mildly Acidic Aqueous Zinc Electrolytes. *Small* **2024**, *20*, 2404583. [CrossRef] [PubMed]
84. Pan, H.; Shao, Y.; Yan, P.; Cheng, Y.; Han, K.S.; Nie, Z.; Wang, C.; Yang, J.; Li, X.; Bhattacharya, P.; et al. Reversible aqueous zinc/manganese oxide energy storage from conversion reactions. *Nat. Energy* **2016**, *1*, 39–51. [CrossRef]
85. Zhu, Y.; Yin, J.; Zheng, X.; Emwas, A.-H.; Lei, Y.; Mohammed, O.F.; Cui, Y.; Alshareef, H.N. Concentrated dual-cation electrolyte strategy for aqueous zinc-ion batteries. *Energy Environ. Sci.* **2021**, *14*, 4463–4473. [CrossRef]
86. Parker, J.F.; Chervin, C.N.; Nelson, E.S.; Rolison, D.R.; Long, J.W. Wiring zinc in three dimensions re-writes battery performance-dendrite-free cycling. *Energy Environ. Sci.* **2014**, *7*, 1117–1124. [CrossRef]
87. Burton, T.F.; Jommongkol, R.; Zhu, Y.; Deebansok, S.; Chitbankluai, K.; Deng, J.; Fontaine, O. Water-in-salt electrolytes towards sustainable and cost-effective alternatives: Example for zinc-ion batteries. *Curr. Opin. Electrochem.* **2022**, *35*, 101070. [CrossRef]
88. Hou, W.; Araujo-Correa, A.E.; Qiu, S.; Velez, C.O.; Acosta-Tejada, Y.D.; Feliz-Hernández, L.N.; González-Nieves, K.; Morell, G.; Piñero Cruz, D.M.; Wu, X. Electrochemical Studies of Metal Phthalocyanines as Alternative Cathodes for Aqueous Zinc Batteries in "Water-in-Salt" Electrolytes. *Batteries* **2025**, *11*, 88. [CrossRef]
89. Shen, Y.; Liu, B.; Liu, X.; Liu, J.; Ding, J.; Zhong, C.; Hu, W. Water-in-salt electrolyte for safe and high-energy aqueous battery. *Energy Storage Mater.* **2021**, *34*, 461–474. [CrossRef]
90. Liu, C.; Xu, W.; Zhang, L.; Zhang, D.; Xu, W.; Liao, X.; Chen, W.; Cao, Y.; Li, M.C.; Mei, C.; et al. Electrochemical Hydrophobic Tri-layer Interface Rendered Mechanically Graded Solid Electrolyte Interface for Stable Zinc Metal Anode. *Angew. Chem. Int. Ed.* **2024**, *63*, e202318063. [CrossRef]
91. Xu, M.; Liu, F.; Chen, L.; Lei, Y.; Liu, Z.; Abdiryim, T.; Xu, F.; You, J.; Tan, Y.; Tan, Z.; et al. Zwitterionic poly(ionic liquid) hydrogel electrolytes with high-speed ion conduction channels for dendrite-free, long-enduring zinc-ion batteries and flexible electronics. *Energy Storage Mater.* **2025**, *80*, 104373. [CrossRef]

92. Peng, H.; Wang, D.; Zhang, F.; Yang, L.; Jiang, X.; Zhang, K.; Qian, Z.; Yang, J. Improvements and Challenges of Hydrogel Polymer Electrolytes for Advanced Zinc Anodes in Aqueous Zinc-Ion Batteries. *ACS Nano* **2024**, *18*, 21779–21803. [CrossRef] [PubMed]
93. Wang, Y.; Li, Q.; Hong, H.; Yang, S.; Zhang, R.; Wang, X.; Jin, X.; Xiong, B.; Bai, S.; Zhi, C. Lean-water hydrogel electrolyte for zinc ion batteries. *Nat. Commun.* **2023**, *14*, 3890. [CrossRef] [PubMed]
94. Radjendirane, A.C.; Sha, F.M.; Ramasamy, S.; Rajaram, R.; Angaiah, S. A Review on Recent Advances and Perspectives in Hydrogel Polymer Electrolytes for Aqueous Zinc-Ion Batteries. *Energy Technol.* **2024**, *12*, 2401105. [CrossRef]
95. Cao, L.; Yang, M.; Wu, D.; Lyu, F.; Sun, Z.; Zhong, X.; Pan, H.; Liu, H.; Lu, Z. Biopolymer-chitosan based supramolecular hydrogels as solid state electrolytes for electrochemical energy storage. *Chem. Commun.* **2017**, *53*, 1615–1618. [CrossRef]
96. Zuo, Y.; Zhang, W.; Wei, M.; Zhang, P.; Zhao, S.; Pei, P.; Qiu, L.; Wang, H.; Meng, Z.; Wang, K. A photonic hydrogel for health self-monitoring of solid-state electrolytes in zinc-air batteries. *Energy Storage Mater.* **2022**, *53*, 136–147. [CrossRef]
97. Gao, J.; Guo, F.; Ji, C.; He, X.; Mi, H.; Qiu, J. A flexible and stable zinc-ion hybrid capacitor with polysaccharide-reinforced cross-linked hydrogel electrolyte and binder-free carbon cathode. *J. Mater. Chem. A* **2022**, *10*, 24639–24648. [CrossRef]
98. He, X.; Zhang, H.; Zhao, X.; Zhang, P.; Chen, M.; Zheng, Z.; Han, Z.; Zhu, T.; Tong, Y.; Lu, X. Stabilized Molybdenum Trioxide Nanowires as Novel Ultrahigh-Capacity Cathode for Rechargeable Zinc Ion Battery. *Adv. Sci.* **2019**, *6*, 1900151. [CrossRef]
99. Gao, C.; Duan, Y.; Liu, Y.; Gu, J.; Guo, Z.; Huo, P. A high energy density supercapacitor fabricated with aqueous polymer electrolyte based on soybean protein isolate grafted by polyacrylic acid. *J. Power Sources* **2022**, *541*, 231658. [CrossRef]
100. Huang, Y.; Zhong, M.; Shi, F.; Liu, X.; Tang, Z.; Wang, Y.; Huang, Y.; Hou, H.; Xie, X.; Zhi, C. An Intrinsically Stretchable and Compressible Supercapacitor Containing a Polyacrylamide Hydrogel Electrolyte. *Angew. Chem. Int. Ed.* **2017**, *56*, 9141–9145. [CrossRef]
101. Yang, S.; Wu, Q.; Li, Y.; Luo, F.; Zhang, J.; Chen, K.; You, Y.; Huang, J.; Xie, H.; Chen, Y. A Bio-Inspired Multifunctional Hydrogel Network with Toughly Interfacial Chemistry for Dendrite-Free Flexible Zinc Ion Battery. *Angew. Chem. Int. Ed.* **2024**, *63*, e202409160. [CrossRef] [PubMed]
102. Xiang, Z.; Li, Y.; Cheng, X.; Yang, C.; Wang, K.-P.; Zhang, Q.; Wang, L. Lean-water hydrogel electrolyte with improved ion conductivity for dendrite-free zinc-Ion batteries. *Chem. Eng. J.* **2024**, *490*, 151524.
103. Yan, H.; Zhang, X.; Yang, Z.; Xia, M.; Xu, C.; Liu, Y.; Yu, H.; Zhang, L.; Shu, J. Insight into the electrolyte strategies for aqueous zinc ion batteries. *Coord. Chem. Rev.* **2022**, *452*, 214297. [CrossRef]
104. Shen, Z.; Liu, Y.; Li, Z.; Tang, Z.; Pu, J.; Luo, L.; Ji, Y.; Xie, J.; Shu, Z.; Yao, Y.; et al. Highly-Entangled Hydrogel Electrolyte for Fast Charging/Discharging Properties in Aqueous Zinc Ion Batteries. *Adv. Funct. Mater.* **2024**, *35*, 2406620.
105. Sun, M.; Ji, G.; Li, M.; Zheng, J. A Robust Hydrogel Electrolyte with Ultrahigh Ion Transference Number Derived from Zincophilic "Chain-Gear" Network Structure for Dendrite-Free Aqueous Zinc Ion Battery. *Adv. Funct. Mater.* **2024**, *34*, 2402004.
106. Zeng, Z.; Liao, S.; Ma, G.; Qu, J. High-Conductivity and Ultrastretchable Self-Healing Hydrogels for Flexible Zinc-Ion Batteries. *ACS Appl. Mater. Interfaces* **2024**, *16*, 58961–58972.
107. Long, J.; Han, T.; Lin, X.; Zhu, Y.; Liu, J.; Niu, J. A quasi-solid-state self-healing flexible zinc-ion battery using a dual-crosslinked hybrid hydrogel as the electrolyte and Prussian blue analogue as the cathode material. *Chem. Sci.* **2024**, *15*, 10200–10206. [CrossRef]
108. Cao, M.; Wang, Y.; Zhang, Y.; Yu, M.; Zhao, Q.; Briscoe, J.; Lu, Y.; Yao, J. Tough and recyclable hydrogel electrolytes with continuous ion migration pathways for dendrite-free zinc-ion batteries under harsh conditions. *J. Mater. Chem. A* **2025**, *13*, 13276–13285.
109. Chen, M.; Zhou, W.; Wang, A.; Huang, A.; Chen, J.; Xu, J.; Wong, C.P. Anti-freezing flexible aqueous Zn–MnO_2 batteries working at −35 °C enabled by a borax-crosslinked polyvinyl alcohol/glycerol gel electrolyte. *J. Mater. Chem. A* **2020**, *8*, 6828–6841. [CrossRef]
110. Wang, Q.; Huang, J.; Qi, L.; Li, M.; Wang, S.; Chen, J.; Sui, Z.; Bi, T.; Tang, Q.; Yu, L.; et al. A Bioinspired Gradient Hydrogel Electrolyte Network with Optimized Interfacial Chemistry toward Robust Aqueous Zinc-Ion Batteries. *ACS Nano* **2025**, *19*, 26770–26781. [CrossRef]
111. Wu, R.; Yang, S.; Wang, R.; Guo, Y.; Du, P. Pullulan enhanced dual-network hydrogel electrolyte for high-performance flexible zinc-ion batteries. *Chem. Eng. J.* **2025**, *509*, 161223. [CrossRef]
112. Du, L.L.; Wang, S.W.; Song, W.J.; Liu, H.; Wang, P.F.; Zhu, M.; Gong, Z.; Zhang, Y.H.; Wu, Y.H.; Shi, F.N. Liquid-permeable and solid-blocking hydrogel barrier layer enables dendrite-free growth of zinc anodes in aqueous zinc-ion batteries. *J. Alloys Compd.* **2025**, *1031*, 180826. [CrossRef]
113. Zhu, Z.X.; Wang, L.X.; Tang, X.N.; Li, L.; Shi, Y.; Shao, J.J. Application of poly(vinyl alcohol) conductive hydrogel electrolytes in zinc ion batteries. *Chin. J. Inorg. Chem.* **2025**, *41*, 893–902.
114. Yu, J.; Li, M.; Kong, X.; Wang, T.; Zhang, H.; Zhu, X.; Zhao, J.; Ma, Z.; Yang, H. Polyanion hydrogel electrolyte with a high Zn^{2+} transference number for dendrite-free aqueous zinc-ion batteries. *J. Mater. Chem. A* **2025**, *13*, 16182–16192. [CrossRef]
115. Chen, Y.; He, S.; Rong, Q. Stretchable, anti-drying, and self-healing hydrogel electrolytes for thermal adaptive zinc–air batteries with robust electrolyte/electrode interfaces. *Mater. Today Chem.* **2023**, *33*, e201726. [CrossRef]

116. Lin, Y.; Wang, S.; Huang, J.; Chen, L.; Bi, T.; Qi, L.; Cai, Z.; Zeng, X.; Hu, P.; Chen, W.; et al. Coupling of Mechanical, Self-Healing, Adhesion, and High-Ion Conducting Properties in Anti-Freezing Hydrogel Electrolytes of Zinc Ion Batteries via Fe^{3+}-Carboxylate Coordination. *Adv. Funct. Mater.* **2025**, *35*, 2504726. [CrossRef]
117. Song, Z.; Liu, X.; Ding, J.; Liu, J.; Han, X.; Deng, Y.; Zhong, C.; Hu, W. Poly(acrylic acid)-Based Composite Gel Polymer Electrolytes with High Mechanical Strength and Ionic Conductivity toward Flexible Zinc-Air Batteries with Long Cycling Lifetime. *ACS Appl. Mater. Interfaces* **2022**, *14*, 49801–49810. [CrossRef]
118. Xu, J.; Zhu, Y.; Gui, Q.; Sun, S.; Zhao, P.; Mao, L.; Luo, T. High-Performance Fatigue-Resistant Dual-Polyrotaxane Hydrogel Electrolytes for Flexible Aqueous Zinc-Ion Batteries. *Small* **2025**, *21*, 2500124. [CrossRef]
119. Wei, T.; Ren, Y.; Li, Z.; Zhang, X.; Ji, D.; Hu, L. Bonding interaction regulation in hydrogel electrolyte enable dendrite-free aqueous zinc-ion batteries from −20 to 60 °C. *Chem. Eng. J.* **2022**, *434*, 134646. [CrossRef]
120. Ji, S.; Luo, H.; Qin, S.; Zhang, X.; Hu, Y.; Zhang, W.; Sun, J.; Xu, J.; Xie, H.; Yan, Z.; et al. Component Fluctuation Modulated Gelation Effect Enable Temperature Adaptability in Zinc-Ion Batteries. *Adv. Energy Mater.* **2024**, *14*, 2400063. [CrossRef]
121. Gao, R.; Wang, J.; Song, Y.; Li, K.; Chen, Z.; Shen, Q.; Wang, Y. Polymer-Salt Effects with Enhanced Eutectic Behavior in Hydrogel Electrolytes for Aqueous Zinc Batteries at −70 °C. *Adv. Funct. Mater.* **2025**, e14585. [CrossRef]
122. Liu, Z.; Zhang, Y.; Li, M.; Li, H.; Zhang, J.; Zhao, Y.; Xu, G.; Hu, J.; Lin, T.; Zhang, N. Lean-Water Gel Electrolyte Enables Zinc Ion Battery at −70 °C. *Angew. Chem. Int. Ed.* **2025**, e202511520. [CrossRef]
123. Ma, B.; Gao, Y.; Miao, L.; Xuan, H.; Tao, X.; Cheng, X.; Shi, P.; Huang, Y.; Zhao, Y.; Shao, Y.; et al. Unraveling the Ultrafast Deposition Kinetics Within Zincphilic and Hydrophobic Organic Interphases for Dendrite-Free and Long Lifespan Zinc Anodes. *Adv. Funct. Mater.* **2025**, e13183. [CrossRef]
124. Wang, D.; Zhao, D.; Chang, L.; Zhang, Y.; Wang, W.; Zhang, W.; Zhu, Q. Interface engineering of electron-ion dual transmission channels for ultra-long lifespan quasi-solid zinc-ion batteries. *Energy Storage Mater.* **2025**, *74*, 103903. [CrossRef]
125. Chen, L.; Xiao, T.; Yang, J.L.; Liu, Y.; Xian, J.; Liu, K.; Zhao, Y.; Fan, H.J.; Yang, P. In-Situ Spontaneous Electropolymerization Enables Robust Hydrogel Electrolyte Interfaces in Aqueous Batteries. *Angew. Chem. Int. Ed.* **2024**, *63*, e202400230. [CrossRef]
126. Liu, B.; Xu, Z.; Wei, C.; Zhu, Z.; Fang, Y.; Lei, X.; Zhou, Y.; Tang, C.; Ni, S.; Pan, H.; et al. Re-understanding and mitigating hydrogen release chemistry toward reversible aqueous zinc metal batteries. *eScience* **2025**, *5*, 100330. [CrossRef]
127. Tan, H.; Meng, C.; Zhang, Y.P.; Zhao, J.Y.; Chen, H.; Chen, L.; Yin, Z.H.; Wu, X.L.; Liu, H.; Wang, J.J. Decoupling of Ion-Solvent Interactions via Compartmentalized Molecular Design for Ultra-Stable Aqueous Zinc Batteries. *Adv. Funct. Mater.* **2025**, e16270. [CrossRef]
128. Liu, T.; Du, X.; Wu, H.; Ren, Y.; Wang, J.; Wang, H.; Chen, Z.; Zhao, J.; Cui, G. A Bio-Inspired Methylation Approach to Salt-Concentrated Hydrogel Electrolytes for Long-Life Rechargeable Batteries. *Angew. Chem. Int. Ed.* **2023**, *62*, e202311589. [CrossRef]
129. Wei, S.; Wang, Y.; Chen, S.; Song, L. Structure regulation and synchrotron radiation investigation of cathode materials for aqueous Zn-ion batteries. *Chem. Sci.* **2024**, *15*, 7848–7869. [CrossRef]
130. Li, G.; Zhao, Z.; Zhang, S.; Sun, L.; Li, M.; Yuwono, J.A.; Mao, J.; Hao, J.; Vongsvivut, J.P.; Xing, L.; et al. A biocompatible electrolyte enables highly reversible Zn anode for zinc ion battery. *Nat. Commun.* **2023**, *14*, 6526. [CrossRef]
131. Han, J.; Jung, S.; Heo, S.E.; Choi, B.; Ryu, S.; Park, S.; Hong, J.; Yoo, J. Anisotropic Ion-Guiding Hydrogel Electrolyte with High-Water Affinity for Zn Ion Battery. *Small* **2025**, *21*, e2500799. [CrossRef]
132. Zhao, Y.; Chen, Z.; Gao, X.; Dong, H.; Zhao, X.; He, G.; Yang, H. In-Situ Self-Respiratory Solid-to-Hydrogel Electrolyte Interface Evoked Well-Distributed Deposition on Zinc Anode for Highly Reversible Zinc-Ion Batteries. *Angew. Chem. Int. Ed.* **2025**, *64*, e202415251. [CrossRef]
133. Li, Y.; Zhang, Y.; Zhao, H.; Li, J.; Xu, H.; Sun, P.; Xu, G.; Li, J.; Pan, L. Unlocking the mysteries of interfacial processes in zinc-ion batteries through multiscale advanced characterization techniques. *Nano Res.* **2025**, e202511520. [CrossRef]
134. Huang, J.; Wang, S.; Yu, L.; Lizundia, E.; Zeng, X.; Chen, L.; Lu, Z.; Qi, L.; Lin, Y.; Deng, H.; et al. Practical, sustainable, wide-temperature-adaptable zinc-metal batteries enabled by electrogelated recyclable biomacromolecular hydrogel electrolytes. *Natl. Sci. Rev.* **2025**, *12*, nwaf308. [CrossRef]
135. Lu, H.; Hu, J.; Wei, X.; Zhang, K.; Xiao, X.; Zhao, J.; Hu, Q.; Yu, J.; Zhou, G.; Xu, B. A recyclable biomass electrolyte towards green zinc-ion batteries. *Nat. Commun.* **2023**, *14*, 4435. [CrossRef]